J. Fluid Mech. (1982), *vol.* 123, *pp.* 91–130
Printed in Great Britain

The forced mixing layer between parallel streams

By D. OSTER† AND I. WYGNANSKI
School of Engineering, Tel-Aviv University, Ramat-Aviv, Tel-Aviv, Israel

(Received 24 September 1980 and in revised form 2 September 1981)

The effect of periodic two-dimensional excitation on the development of a turbulent mixing region was studied experimentally. Controlled oscillations of variable amplitude and frequency were applied at the initiation of mixing between two parallel air streams. The frequency of forcing was at least an order of magnitude lower than the initial instability frequency of the flow in order to test its effect far downstream. The effect of the velocity difference between the streams was also investigated in this experiment. A typical Reynolds number based on the velocity difference and the momentum thickness of the shear layer was 10^4.

It was determined that the spreading rate of the mixing layer is sensitive to periodic surging even if the latter is so small that it does not contribute to the initial energy of the fluctuations. Oscillations at very small amplitudes tend to increase the spreading rate of the flow by enhancing the amalgamation of neighbouring eddies, but at higher amplitudes the flow resonates with the imposed oscillation. The resonance region can extend over a significant fraction of the test section depending on the Strouhal number and a dimensionless velocity-difference parameter. The flow in the resonance region consists of a single array of large, quasi-two-dimensional vortex lumps, which do not interact with one another. The exponential shape of the mean-velocity distribution is not affected in this region, but the spreading rate of the flow with increasing distance downstream is inhibited. The Reynolds stress in this region changes sign, indicating that energy is extracted from the turbulence to the mean motion; the intensity of the spanwise fluctuations is also reduced, suggesting that the flow tends to become more two-dimensional.

Amalgamation of large coherent eddies is resumed beyond the resonance region, but the flow is not universally similar. There are many indications suggesting that the large eddies in the turbulent mixing layer at fairly large *Re* are governed by an inviscid instability.

1. Introduction

The significance of the mixing layer in many engineering applications is well recognized. It dominates the initial flow patterns in jets and in wakes caused by bluff bodies; it governs the flow field in combustion chambers and flow reactors whose size or efficiency depend on the rate of mixing (Hill 1976). It is also recognized that most of the noise associated with jet propulsion originates in the mixing layer (Liu, Alper & Mankbudi 1978; Moore 1978; Ffowcs Williams & Kempton 1978).

The first comprehensive investigation of the mixing layer generated by a single stream discharging into quiescent surrounding fluid was made by Liepmann & Laufer (1947), who proved that the flow is self-preserving. Self-preservation implies that all

† Present address: Department of Aerospace Engineering, University of Southern California, Los Angeles, California 90007.

important parameters of the flow are independent of Reynolds number and become similar when rendered dimensionless through division by a single velocity and lengthscale. Self-preservation also implies that 'a moving equilibrium is set up in which conditions at the initiation of the flow are highly irrelevant...' (from Townsend 1976, p. 196). The mixing layer investigated by Wygnanski & Fiedler (1970) also appeared to be self-preserving, but its rate of spreading in the streamwise direction was approximately 30 % larger than previously reported. The new result, barring the possibility of an experimental error, cast some doubts about the attainment of Reynolds-number similarity below $R = Ux/\nu = 10^6$, or the universality of the concept of self-preservation. Wygnanski & Fiedler alluded to the possibility that a trip wire that they had placed on the splitter plate was responsible for the different rate of growth of their flow, but Batt (1975) actually proved that a trip wire enhanced the rate of growth of the mixing layer. The sensitivity of the turbulent mixing layer to a variety of experimental conditions became a subject of discussion in the literature, it is mentioned by Brown & Roshko (1974), Champagne, Pao & Wygnanski (1976), Dimotakis & Brown (1976), Foss (1977), Birch (1977), Oster *et al.* (1978), Hussain & Zedan (1978*a*, *b*) and Browand & Latigo (1979), to mention a few.

The existence of large coherent eddies in a plane turbulent mixing layer was first reported by Brown & Roshko (1971) on the basis of flow visualization. Analysis of motion pictures enabled the authors to observe a reduction in the eddy-passage frequency with increasing downstream distance as a result of merging interactions among adjacent eddies (Brown & Roshko 1974). Winant and Browand (1974) observed that adjacent vortices tend to roll around each other before merging and generating a larger vortex. They called the process 'vortex pairing' and claimed that it is responsible for the growth of the mixing layer. The pairing process occurs randomly in space and time, resulting in a linear continuous growth of the shear layer with increasing downstream distance. Hernan & Jimenez (1979) analysed digitally Brown & Roshko's (1974) ciné film and attributed most of the growth of the mixing layer to the growth of the large coherent eddies rather than to the amalgamation process (see also Oster *et al* 1978). Since the amount of information available is rather limited, additional proof is necessary to support their conclusion.

The presence of large coherent eddies as part and parcel of a fully developed turbulent mixing layer is not universally accepted. Chandrsuda *et al.* (1978) suggest that these vortices are but a relic of transition and can only be seen whenever the free-stream turbulence level is very low; in less-favourable conditions the flow develops into the classical, chaotic three-dimensional turbulence. Pui & Gartshore (1979) suggested that the large coherent structures result from vibrating apparatus; in particular, a vibrating splitter plate appeared to be responsible for the generation of large eddies, which disappeared when the vibration was eliminated by external means.

The hyper-sensitivity of the mixing layer to the experimental conditions and apparatus can be understood more easily if one accepts the existence of the orderly coherent structures in this flow. Small perturbations in the direction normal to the stream may displace an eddy, causing it to roll around its neighbour and eventually amalgamate with it. These perturbations may be initiated anywhere in the flow. In the free stream, they may be caused by fan-blade passage frequency (Fiedler & Thies 1978), vibrations, or a high level of turbulence resulting from lack of adequate screens or contraction. They may also be caused by a feedback mechanism (Dimotakis & Brown 1976, Ho & Nosseir 1981) resulting from earlier eddy dislocations and interactions. The flow appears to be most susceptible to perturbations introduced at

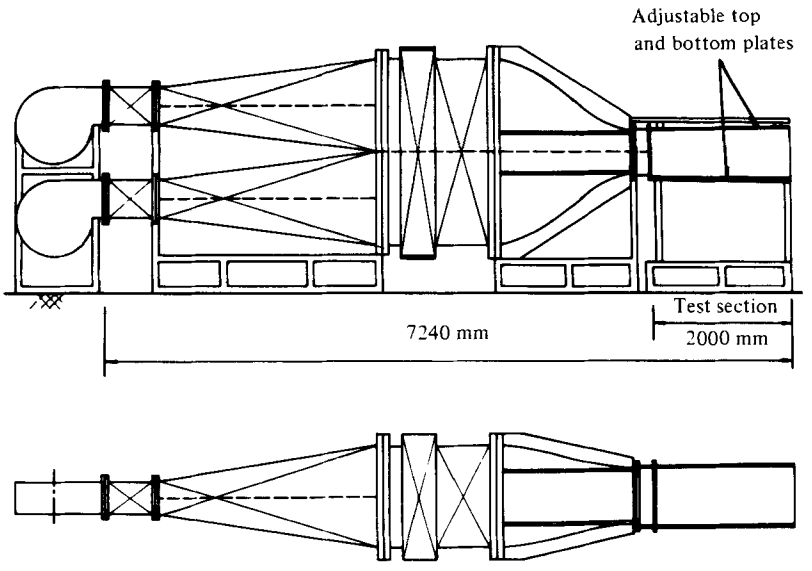

FIGURE 1. The wind tunnel.

the initiation of mixing, i.e. in the neighbourhood of the splitter plate. Vortices shed from a trip wire may cause oscillations that trigger the natural instability of the mixing layer, changing its rate of growth. Turbulence generated in the upstream boundary layers has a similar effect on the spreading rate of the shear layer (Browand & Latigo 1979; Hussain & Zedan 1978*a*, *b*).

However, fixed disturbances like trip wires or vortex generators introduce a complicated spectrum of perturbations into the flow, which are not easily amenable to analysis. Thus the purpose of the present investigation is to examine and possibly exploit the sensitivity of the turbulent shear layer to small-amplitude, controlled, two-dimensional oscillations introduced at the origin of the flow.

2. Apparatus and experimental procedures

2.1. *The wind tunnel*

The apparatus consisted of two independent cascade blower tunnels discharging into a common test section (figure 1). The two tunnels, which were mirror images of one another, were separated intially by a splitter plate that extended upstream through the contraction section and into the settling chamber. The splitter plate ended 20 cm downstream of the contraction, allowing the two streams to become parallel before the initiation of mixing. The trailing edge of the splitter plate was milled at an included angle of 3°.

Each tunnel consisted of a backward-facing-step blower supplying the air, a diffuser, a settling chamber and a contraction. The blowers were vibration-isolated from the rest of the structure and equipped with filters at the inlet. A small settling chamber and a gauze were situated between the blower and the diffuser in order to provide resistance and equalize spatially the flow entering the diffuser. Each diffuser was subdivided into four smaller channels having an equivalent cone angle smaller than 5°. A deep honeycomb and 3 turbulence-damping screens were installed in the settling chamber. The contraction ratio of the nozzle was 7·3:1. The test section was 2000 mm long, 500 mm high and 600 mm wide. The turbulence level at the nozzle

exit was 0·2 % and the mean velocity variation across the test section was less than 1 % outside of the boundary layers. The top and bottom walls of the test section were mounted on screw jacks, enabling adjustment and the elimination of streamwise pressure gradient. These walls were readjusted whenever the velocity ratio between the two streams was changed. For the series of tests reported here the velocity of the lower stream was maintained at 13·5 m/s, while the velocity of the upper stream could vary between 0 and 13·5 m/s.

The measuring sensors were mounted on a traversing gear, which had three degrees of freedom: translation in the x- and y-directions and rotation about the y-axis. The rotation of the sensors was essential for calibration of x-array hot-wires. The translation in the streamwise direction was manual, with a resolution of 1 mm, the motion of the y-direction was computer controlled, with a resolution distance of 0·02 mm. The angular motion was also computer controlled, with a resolution of 1·08°.

2.2. *The disturbance generator and instrumentation*

A thin flap pivoted at its leading edge generated the required perturbations. The flap was 10 mm wide and 0·5 mm thick and spanned the entire test section along the trailing edge of the splitter plate. The gap between the splitter plate and the flap was sealed by an adhesive tape. The sinusoidal oscillations were provided by two voice coils, which were activated by a function generator. The motion of the flap was monitored optically during the experiment using stroboscopic illumination and a theodolite.

Constant-temperature hot-wire anemometers were used throughout the investigation. The sensors were mounted in rakes spanning at times the entire cross-section of the flow. The wire was made of tungsten, 5 μm in diameter, which was welded to the prongs. The frequency response, as determined by a square-wave method, was approximately 10 kHz.

Hot-wire calibration and the acquisition of data were done digitally using a PDP 11/60 minicomputer. The analog-to-digital converter had a 12 bit precision, amounting to a resolution of 4096 steps. The signals were sampled at a rate of 4000 samples/s per channel, converted to velocities by using calibration constants and stored on digital tape for further processing.

2.3. *Calibration procedure*

The use of the computer for data acquisition both simplifies and shortens the calibration procedure, enabling the simultaneous use of an array of sensors (Wygnanski 1978). The calibration of a normal wire can be obtained, either by fitting a curve to a set of calibration velocities, or by generating a look-up table for all possible velocities. In this experiment the velocity–voltage relationship was assumed to follow a 4th-order polynomial so that the velocity of the ith wire is given by

$$U_i = \sum_{k=0}^{4} a_{ik} E_i^k .$$

Whenever more than 5 calibration velocities were used a 4th-order polynomial was fitted to the data by a method of least squares.

The calibration of an x-array is somewhat more complicated, because the response of each wire in the array depends on the velocity vector Q and its inclination angle α to the stem of the probe.

Thus the response of each wire in the x-array is given by $E_1 = E_1(Q,\alpha)$ and $E_2 = E_2(Q,\alpha)$, where E_1 and E_2 are single-valued functions in the range under consideration. It is assumed that Q and α may be determined uniquely from a pair

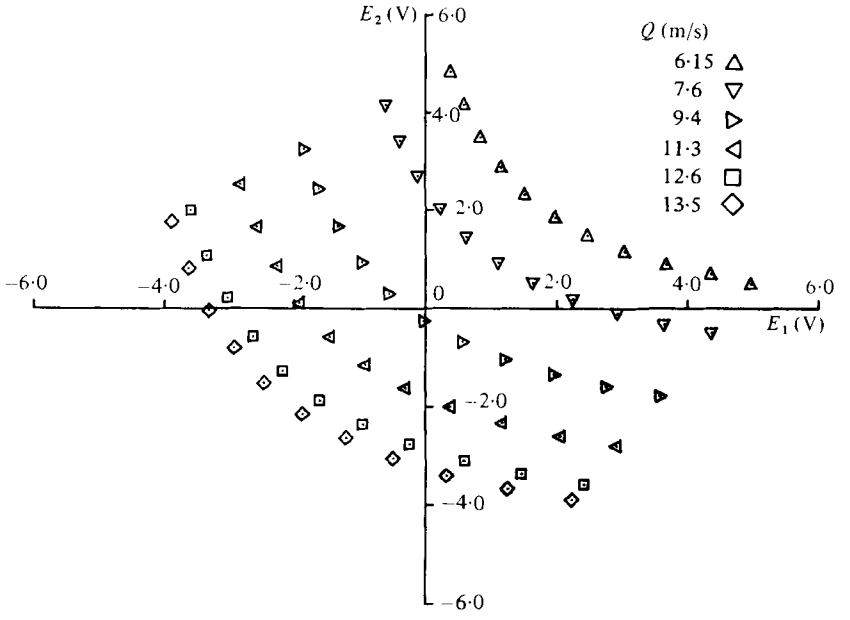

FIGURE 2. Calibration voltages for an x-array wire.

of voltages E_1 and E_2, so that $Q = Q(E_1, E_2)$ and $\alpha = \alpha(E_1, E_2)$, where the streamwise component of velocity is given by $U = Q\cos\alpha$ and the normal component by $V = Q\sin\alpha$. The calibration procedure requires variation of velocities and inclination angles. Six velocities covering the entire range anticipated in a given experiment were chosen, and at each velocity the probes were yawed 11 times to cover the angles $-27° < \alpha < 27°$. A typical calibration plot in the (E_1, E_2)-plane is shown in figure 2. Q and α are recovered from a pair of signals E_1 and E_2 by fitting a third-order surface to the calibration data, i.e.

$$Q = a_1 E_1^3 + a_2 E_1^2 E_2 + a_3 E_1 E_2^2 + \ldots + a_8 E_1 + a_9 E_2 + a_{10},$$
$$\alpha = b_1 E_1^3 + b_2 E_1^2 E_2 + b_3 E_1 E_2^2 + \ldots + b_8 E_1 + b_9 E_2 + b_{10}.$$

The coefficients of the surface were computed by a least-square fit to the 66 calibration points. The fit was checked for each pair of calibration voltages, and was accepted only after it was established that the error in U was less than 1 % and in V less than 2 %. The larger error in V results from the fact that the maximum error in α was approximately 0·5°. The two sets of coefficients were stored for use during the acquisition of data. Care was taken to recalibrate the anemometers whenever the temperature change approached 1 °C. Periodic checks were made to verify that no data point exceeded the calibration range.

3. Presentation and analysis of the data

3.1. *The unforced mixing layer*

The mean-flow field and the streamwise component of the turbulent intensity were measured in the absence of forcing in order to check the apparatus and obtain a basis for comparison. Most of the measurements were made with normal wires at velocity ratios $r = U_1/U_2 = 0{\cdot}3$, 0·4, 0·5, 0·6, corresponding to a parameter $\lambda = (U_2 - U_1)/(U_2 + U_1) = 0{\cdot}54$, 0·43, 0·33, 0·25 respectively. Here U_1 is the velocity

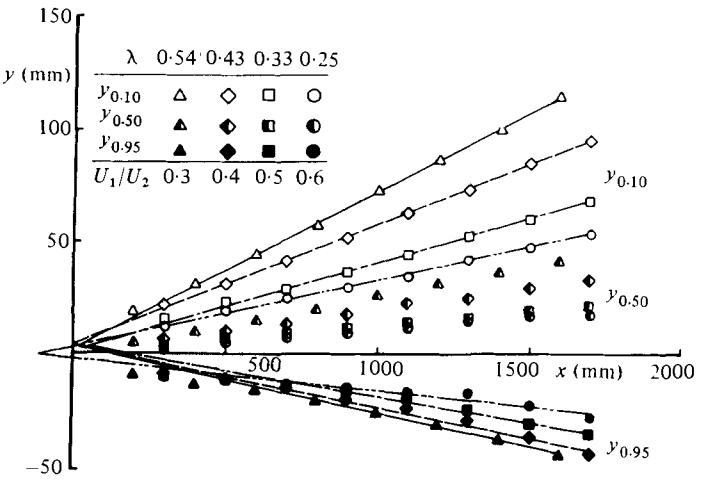

FIGURE 3. The spreading of the unforced mixing layer.

of the low-speed stream and U_2 is the velocity of the high-speed stream. At $r = 0{\cdot}6$ ($\lambda = 0{\cdot}25$) all three components of the turbulent fluctuations and the Reynolds stress were measured.

Since the velocity in the shear layer has to blend with U_1 on the low-speed and with U_2 on the high-speed side of the flow, it has become customary (Liepmann & Laufer 1947; Champagne *et al.* 1976; Birch 1980) to identify some specific y-co-ordinates at which the velocity deviates by a given percentage from the velocity difference between the two streams; e.g. $y_{0\cdot1}$ corresponding to the location at which $\overline{U} = U_1 + 0{\cdot}1(U_2 - U_1)$, or $y_{0\cdot95}$ corresponding to the location at which $\overline{U} = U_1 + 0{\cdot}95(U_2 - U_1)$, where y is the lateral co-ordinate in a Cartesian system measured from the trailing edge of the splitter plate. A constant slope of these loci, when plotted against x-distance from the splitter plate, implies (in general) that the mean-velocity profiles are similar. This is also the case in the present investigation (figure 3) for $x > 700$ mm. The local width b of the mixing layer may be defined as $b = y_{0\cdot1} - y_{0\cdot95}$, and the rate of growth of the mixing layer $db/dx = (y_{0\cdot1} - y_{0\cdot95})/(x - x_0)$, where x_0 is the streamwise distance between the virtual origin of the flow and the trailing edge of the splitter plate. It is obvious that the rate of growth of the shear layer increases with increasing λ mostly owing to the increase in slope of $y_{0\cdot1}$, implying that an increase in the velocity difference between the two streams causes the shear layer to spread more rapidly into the low-speed region. Since the roll up of the vortex sheet into discrete lumps depends on the velocity difference between the streams, this result could be considered to be indirect evidence for the existence of large coherent structures in the mixing layer. The rate of growth db/dx of the shear layer increases linearly with λ (figure 4), and compares favourably with other known results. The large scatter in the data presented in figure 4 is attributed to a variety of reasons, most of which are still to be explored. A partial random list of possibilities is, however, in order:

(i) turbulence in the free stream (Chandrsuda *et al.* 1978);

(ii) oscillations in the free stream resulting from organ-pipe frequency and fan-blade passage (Fiedler & Thies 1978);

(iii) aspect ratio (i.e. the ratio of height to width);

(iv) length of test section (i.e. the interaction of the shear layer with the walls);

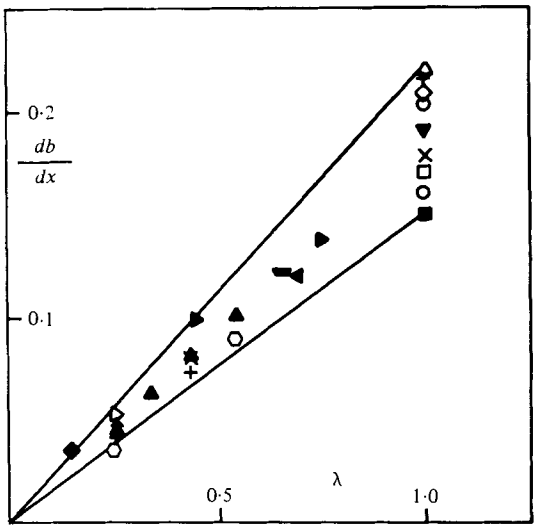

FIGURE 4. Variation of db/dx versus λ: △, Wygnanski & Fiedler (1970); □, Liepmann & Laufer (1947); ▼, Patel (1973); ◇, Champagne *et al.* (1976); ■, Reichardt (1951); ○, Spencer & Jones (1971); ◆, Pui & Gartshore (1979); ▬, Dimotakis & Brown (1976); ×, Oster *et al.* (1977) untripped; +, Oster *et al.* (1977) tripped; ▶, Brown & Roshko (1974); ◀, Browand & Latigo (1979); ▷, Yule (1971); ○, minimum and maximum values from Hussain & Zedan (1978*a*, *b*); ▲, present results.

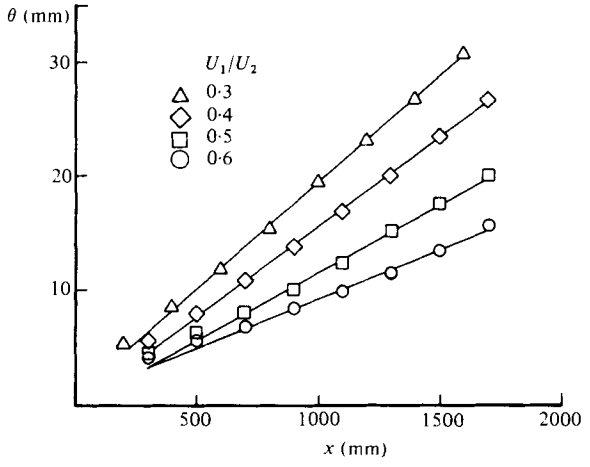

FIGURE 5. Variation of the momentum thickness for the unforced mixing layer.

(v) residual pressure gradients (Browand & Latigo 1979);

(vi) vibration of the splitter plate (Pui & Gartshore 1979);

(vii) the structure of the boundary layer on the splitter plate and the level of the turbulent fluctuations (Hussain & Zedan 1978*a*, *b*, Browand & Latigo 1979);

(viii) the curvature and angle between the merging streams (Batt 1975);

(ix) Reynolds number (Hussain & Zedan 1978*a*).

This scatter, however, gave the impetus to the present investigation and the investigation of Dziomba (1981) into some of the other factors in this list.

Perhaps a better definition of local width of the mixing layer, which is independent

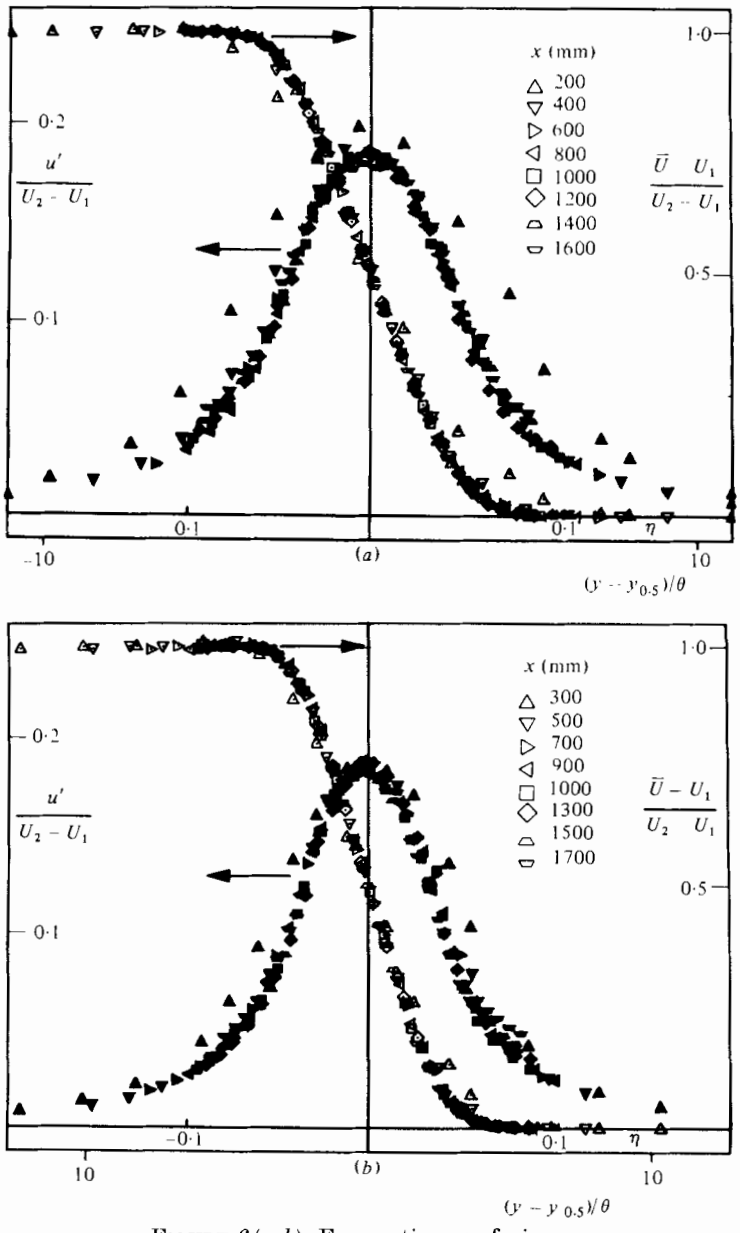

FIGURE 6(*a*, *b*). For caption see facing page.

of the similarity of the velocity profiles at various streamwise distances, is provided by the momentum thickness defined by

$$\theta = \int_{-\infty}^{\infty} \frac{\bar{U} - U_1}{U_2 - U_1}\left[1 - \frac{\bar{U} - U_1}{U_2 - U_1}\right] dy.$$

The dependence of θ (or b) on x does not provide information about possible undulations of the free shear layer. θ, like b, increases linearly with x (figure 5) in the unperturbed shear layer.

The mean-velocity profiles and the streamwise component of the turbulent fluctuations shown in figure 6 suggest that the flow is self-preserving for all 4 velocity

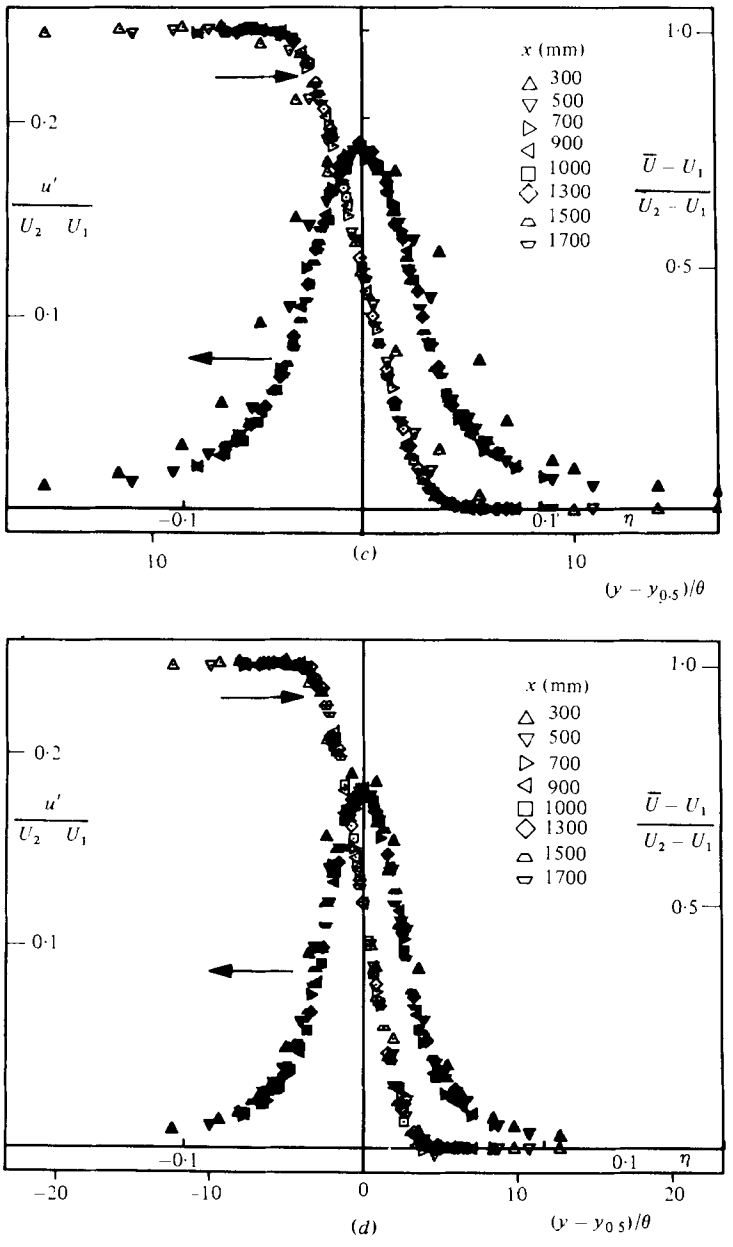

FIGURE 6. The mean-velocity profile and the distribution of $u'/(U_2 - U_1)$: (*a*) $r = 0{\cdot}3$, $f = 0$. (*b*) 0·4, 0. (*c*) 0·5, 0. (*d*) 0·6, 0.

ratios under consideration, provided that $x > 500$ mm. The maximum intensity of the streamwise component u' of the fluctuations, when rendered dimensionless by the velocity difference, is approximately a constant, independent of the velocity ratio (i.e. $u'/(U_2 - U_1) = 0{\cdot}18$), but the lateral of the distribution of this variable in the similarity co-ordinate $\eta = (y - y_{0.5})/(x - x_0)$ becomes narrower with increasing $r = U_1/U_2$. The other components of turbulent intensity v' and w' in the y- and z-directions respectively, as well as the shear stress $\overline{uv}$, were measured for $r = 0{\cdot}6$ only (figure 7). The additional data suggest that the flow is, indeed, self-preserving.

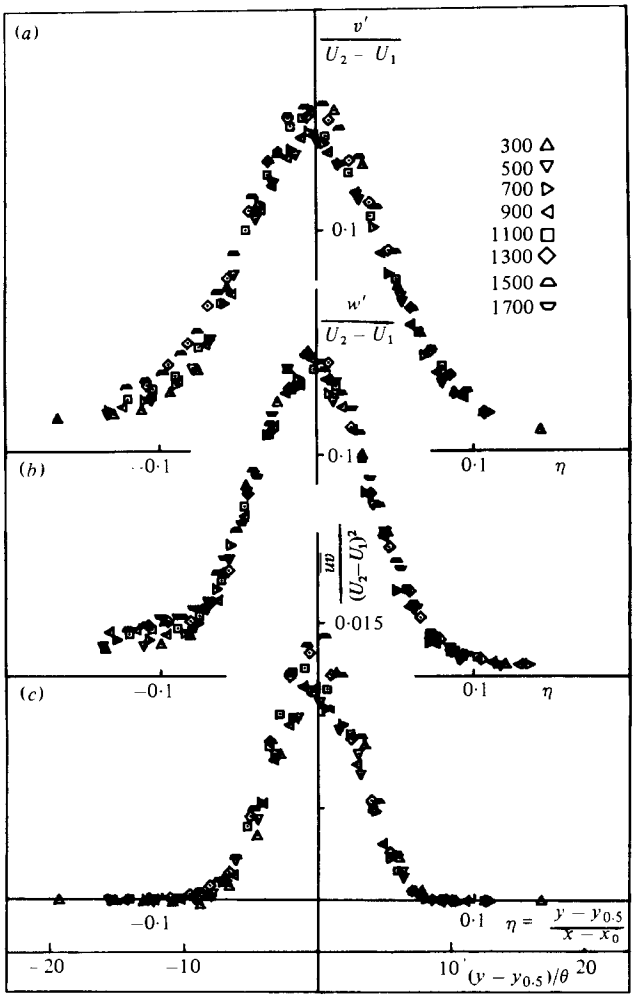

FIGURE 7. Distribution of (a) $v'/(U_2-U_1)$, (b) $w'/(U_2-U_1)$, (c) $\overline{uv}/(U_2-U_1)^2$; all at $r = 0{\cdot}6$, $f = 0$.

There is every reason to believe that for $r < 0{\cdot}6$ the flow remains self-preserving because the Reynolds number based on the velocity difference and a local width ($R = (U_2-U_1)\theta/\nu$) increases with increasing λ (or decreasing r), and Reynolds-number similarity is a pre-requisite for self-preservation. When the maximum values of the turbulent intensity measured at $r = 0{\cdot}6$ by different investigations, are compared (table 1) the discrepancies are quite obvious. The maximum value of $\overline{uv}$ measured here agrees with the results of Yule (1971), while the value of w' agrees with the measurements of Spencer (1970), and differs from the value measured by Yule.

3.2. *The initial conditions in the forced and the unforced shear layers*

The mixing layer is regarded theoretically as an exercise in 'smoothing of a discontinuity' in which two parallel and semi-infinite streams having a different but constant velocity throughout are brought together by some magic device. In reality, however, the two streams are initially separated by a solid surface, which generates

a boundary layer as a result of the no-slip condition at the wall. Even in laminar flow the problem is far from being trivial because of the singular point corresponding to the trailing edge of the solid surface. The existence of the trailing edge affects the boundary layers upstream as well as the evolution of the near wake downstream (Goldstein 1930). The finite thickness of the splitter plate represents an added difficulty. The problems multiply when one considers a tripped boundary layer. The resulting flow, in this case, is seldom a fully developed classical turbulent boundary layer, evolving over a flat surface in absence of pressure gradient, but rather a complicated unknown flow because, in most experimental arrangements, the splitter plate ends a short distance downstream of a contraction.

Some of these difficulties may be avoided by considering the initial conditions some distance downstream (i.e. in the mixing layer itself) after the wake component resulting from the boundary layers has disappeared. The initial conditions were thus carefully examined 100 mm downstream of the splitter plate. The effects of forcing by activating the flap are of particular interest, in order to assess the disturbance level required to affect the development of the shear layer.

Source	$u'/\Delta U$	$v'/\Delta U$	$w'/\Delta U$	$\overline{uv}/(\Delta U)^2$
Spencer (1970)	0·17	0·14	0·145	0·011
Yule (1971)	0·173	0·16	0·18	0·013
Present results	0·180	0·153	0·145	0·013

TABLE 1

The velocity profiles shown in figure 8 were all measured at a fixed velocity ratio ($r = 0{\cdot}6$) at $x = 100$ mm. The forcing frequency was held constant, $f = 30$ Hz, while the maximum amplitude of the excursions of the flap varied from 0 to 1·5 mm. The initial mean-velocity profile is not affected by the motion of the flap (figure 8*a*). Repeating the measurements at higher frequencies, $f = 40$, 50 Hz, did not produce a noticeable change in the lateral velocity distribution.

There is no obvious increase in the turbulent intensity resulting from forcing, as may be seen from the lateral distribution of u' and v' shown in figures 8(*b*, *c*). The only difference was sensed for $f = 60$ Hz and $A = 1{\cdot}5$ mm, where a small increase in u' and a concomitant small decrease in v' were detected. These observations are not limited to $x = 100$ mm only, since the same behaviour was observed at $x = 50$ mm, in spite of the fact that the mean-velocity profile contained a significant wake component. It is particularly interesting to note that the intensity v' does not change with increasing amplitude of the flap's oscillations. The lack of visible effect is contrary to expectations, because the flap, which oscillates in the y-direction, feeds energy directly into the lateral component of the fluctuations. Measurements made further downstream in a different experiment (Wygnanski, Oster & Fiedler 1979) showed a dramatic increase in the intensity of v' as a result of forcing. It was concluded that *the oscillations of the flap have no significant effect on the initial velocity distribution nor on the total turbulent energy present in the flow at* $x = 100$ mm. Neverthless, the forced oscillations caused remarkable differences in the development of the mixing layer further downstream (Oster *et al.* 1978). The effect of forcing can only be understood if it triggers an instability existing naturally in the flow. In this sense, the periodic surging produced by the flap is conceptually different from the

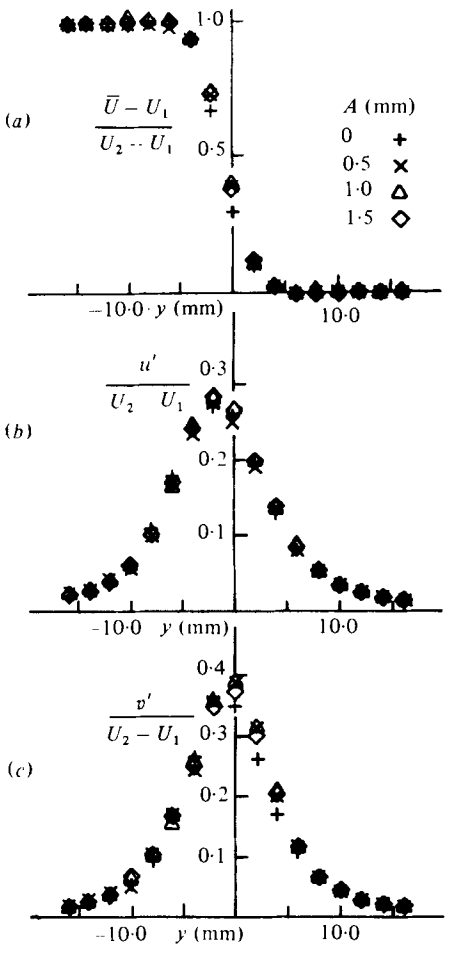

FIGURE 8. Initial conditions; $r = 0{\cdot}6$, $f = 30$ Hz, $x = 100$: (*a*) mean-velocity profiles; (*b*) streamwise velocity fluctuations; (*c*) lateral velocity fluctuations.

periodic forcing imposed on a jet column by Crow & Champagne (1971). In the latter experiment, the r.m.s. fluctuation level of the entire stream was raised to 2%, while in the present case the additional energy is indistinguishable even in the initial mixing layer itself.† How then does the flap work? A partial answer to this question may be given by considering the spectral distribution of the fluctuations for various amplitudes of forcing (figure 9). The data shown were taken directly downstream of the splitter plate ($y = 0$) at $r = 0{\cdot}6$ and frequency $f = 60$ Hz. In the absence of forcing most of the energy is concentrated in a relatively broad-band spectrum at $400 < f < 600$ corresponding to $f\theta_i/(U_2 + U_1) \approx 0{\cdot}02$, since $\theta_i \approx 1$ mm. (Oster, Wygnanski & Fiedler 1977). One may also distinguish a peak in the spectrum at $f = 230$, which is a sub-harmonic of the shedding frequency in the immediate neighbourhood of the trailing edge. With increasing amplitude of the surging (figures 9*c*, *d*) one may note a marked increase in the energy content at the forcing frequency ($f = 60$ Hz) and a relative reduction at high frequencies, so that the integral of all spectral components of u remains approximately constant. Further investigation is required

† A recent paper by Zaman & Hussain indicates that the suppression of turbulence in free shear flows can depend on the forcing method (see Zaman & Hussain 1981, p. 144, figure 7*e*).

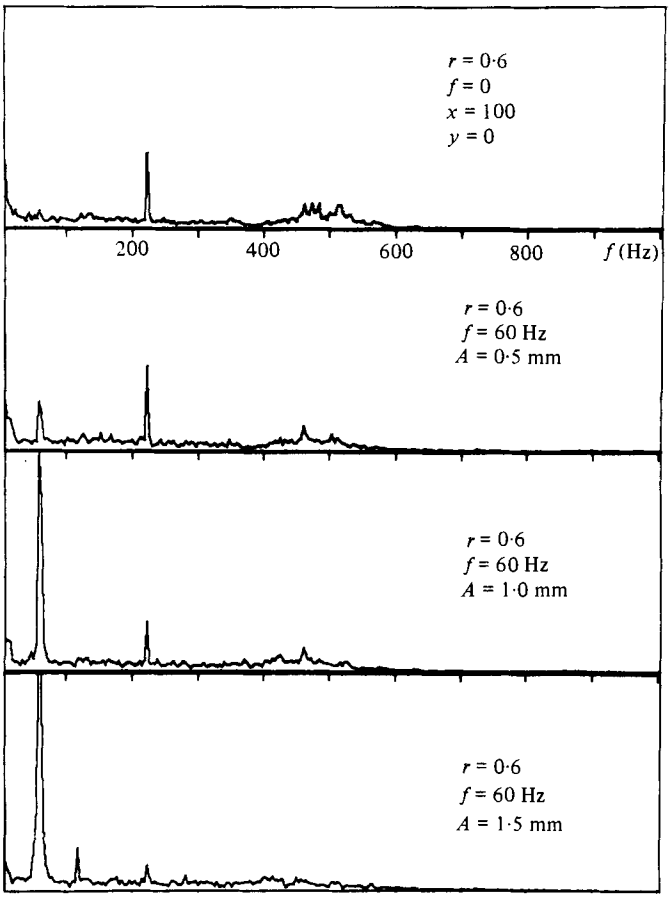

FIGURE 9. Power spectra of the streamwise velocity fluctuations at $x = 100$ mm.

to determine how the fluctuating energy shifts to the forcing frequency, but it is quite possible that the long wave, associated with the low-frequency forcing, causes a large number of small vortices naturally shed at the trailing edge to coalesce. The amalgamation is enhanced during one part of the forced cycle and is impeded during another; the process that was observed by Ho & Nosseir (1978) and Zaman & Hussain (1980) was referred to, by the former authors, as 'collective interaction'. The frequency and amplitude of the flap controls the number of vortices that may have been lumped together, near the trailing edge, into a large coherent eddy. In this way, the relatively slow process in which 2 vortices pair after a protracted interaction may be bypassed.

3.3. *The spreading rate of the forced shear layer*

The activation of the flap influences the development of the mixing layer far downstream. The rate of growth at $r = 0{\cdot}4$ and forcing frequency $f = 40$ Hz is compared with the unforced rate of growth in figure 10. The mixing layer no longer grows linearly with increasing x; it is possible that it grows in an oscillatory fashion, but this possibility was not explored, in view of the limited size of the test section. One may, however, clearly distinguish 3 regions in the streamwise development of the flow:

Region I: in which the initial rate of growth of the forced mixing layer exceeds the

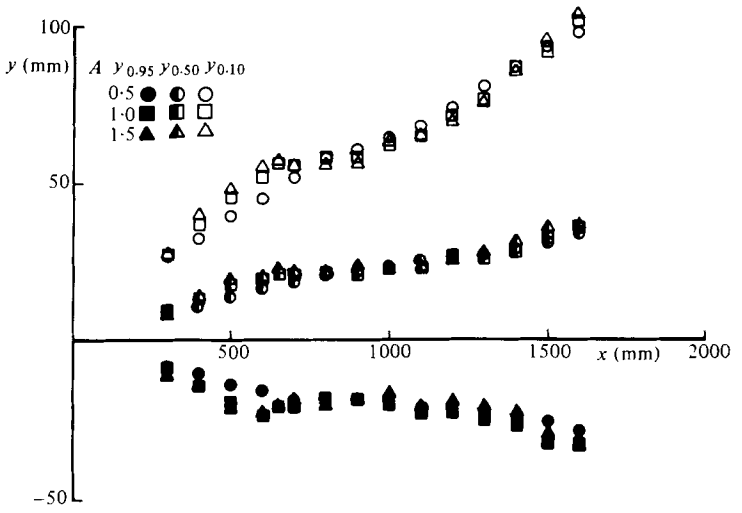

FIGURE 10. Spreading of the forced mixing layer at $r = 0{\cdot}4$, $f = 40$ Hz.

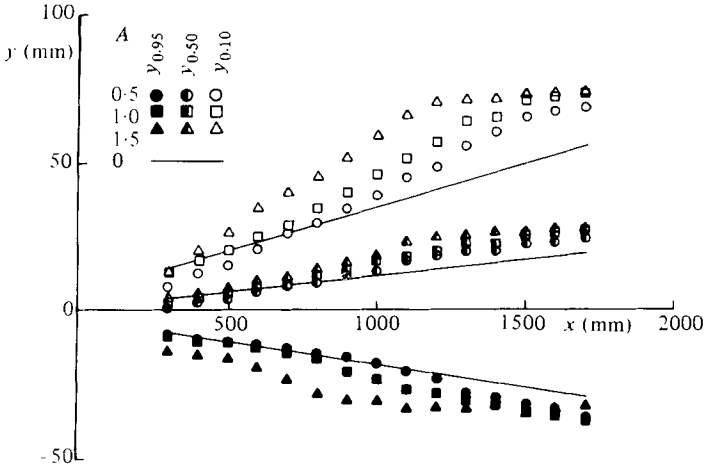

FIGURE 11. Spreading of the forced mixing layer at $r = 0{\cdot}6$, $f = 40$ Hz.

linear growth in the natural case. An increase in the amplitude of forcing in this region results in an enhanced rate of growth of the mixing layer (figure 10).

Region II: in which the rate of growth with increasing x slows or stops, and under extreme conditions of large-amplitude forcing may even become negative. Only for the smallest amplitudes of forcing ($A = 0{\cdot}5$ mm in figure 10) did the growth of the mixing layer not saturate in this region. At the end of region II corresponding to $1200 > x > 800$ mm the width of the mixing layer becomes independent of the amplitude of forcing, and at $1100 < x < 1200$ the width of the flow approaches the width corresponding to the unforced flow condition.

Region III: in this region the mixing layer resumes its rapid downstream growth at almost the same rate as the initial rate of growth in region I.

By increasing the velocity ratio to $r = 0{\cdot}6$ while keeping the velocity of the high-speed fixed and retaining the same forcing frequency and amplitude as before (i.e. $f = 40$, $A = 0{\cdot}5$, $1{\cdot}0$, $1{\cdot}5$ mm) the length of region I increases (figure 11). Thus

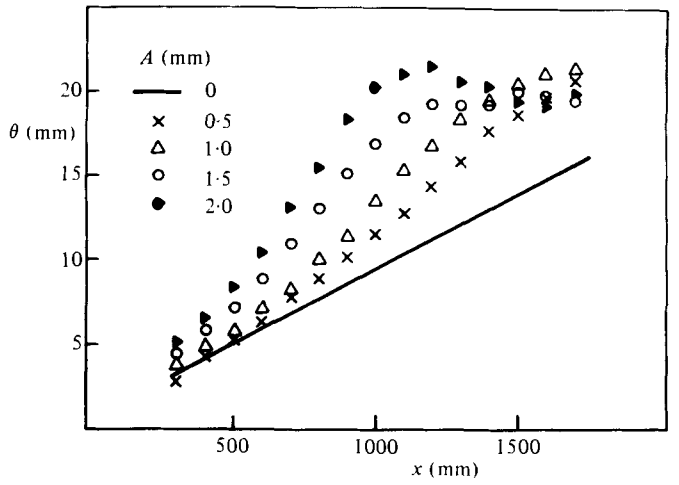

FIGURE 12. Variation of the momentum thickness at $r = 0{\cdot}6$, $f = 40$ Hz.

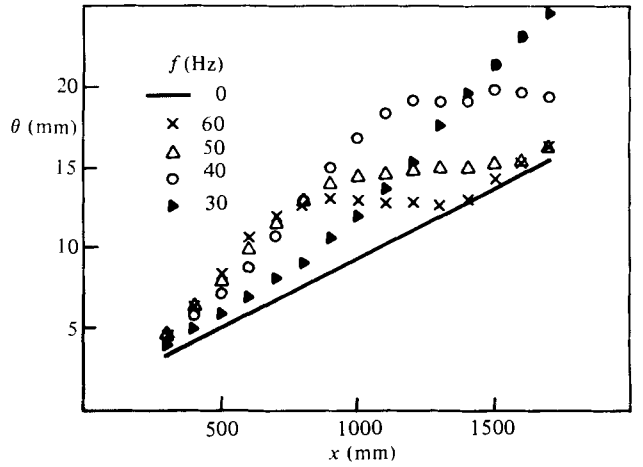

FIGURE 13. Variation of the momentum thickness for forced mixing layers at $r = 0{\cdot}6$, $A = 1{\cdot}5$ mm and 60 Hz $> f >$ 30 Hz.

the transition to region II for $A = 1{\cdot}5$ mm occurs at $x = 1200$ mm, while for $r = 0{\cdot}4$ and identical amplitude and frequency it occurs roughly at $x = 600$ mm. The transition to region III does not occur within the test section. The forced shear layer at the end of region I for $r = 0{\cdot}6$ and $A = 1{\cdot}5$ mm is 70 % wider than the corresponding unforced flow. This number can be significantly exceeded by optimizing the choice of variables to suit a particular velocity ratio and geometry. The local width of the shear layer (at fixed x) depends on the velocity ratio r; and on the forcing frequency and amplitude. The dependence of the momentum thickness θ on the amplitude of forcing at given U_1/U_2 and f is shown in figure 12, where the amplitude is a parameter. The maximum slope of θ increases with increasing A (in region I) but the mixing layer stops growing at smaller values of x; for $A = 2$ mm $d\theta/dx$ becomes negative at $x = 1200$ mm. Thus it is possible that the width of the shear layer diminishes in region II at high amplitude of forcing. The effect of the forcing frequency on the streamwise evolution of the momentum thickness is presented in figure 13 for a constant

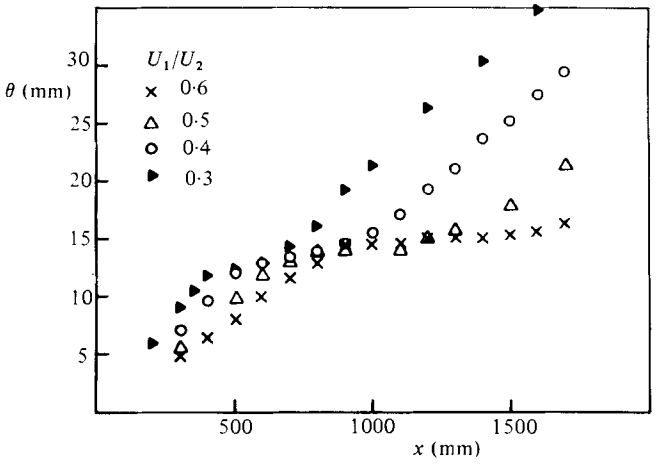

FIGURE 14. Variation of the momentum thickness for forced mixing layers at $f = 50$ Hz, $A = 1{\cdot}5$ mm and $0{\cdot}6 > r > 0{\cdot}3$.

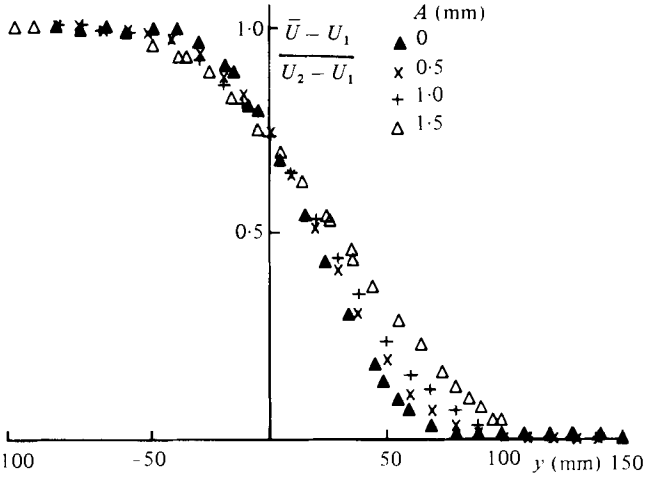

FIGURE 15. Effect of amplitude on the mean velocity; $r = 0{\cdot}6$, $f = 30$ Hz, $x = 1700$, $A = 0{\cdot}5$, 1·0, 1·5 mm.

amplitude of forcing ($A = 1{\cdot}5$) and a constant velocity ratio. In figure 14 the velocity ratio varies between $0{\cdot}6 > r > 0{\cdot}3$, with all the other parameters unchanged. The length of region I appears to be inversely proportional to the surging frequency, provided that all other variables remain constant. The length of region I at a fixed forcing frequency decreases with r. It is believed that the length of region II behaves in a similar manner; however, the dependence on r can be clearly observed in figure 14, while the dependence on f is only observed at $f = 50$ and 60 Hz, because the length of the test section is a limiting factor. The slope $d\theta/dx$ is not necessarily constant in region I, and it tends to increase with increasing x (e.g. $r = 0{\cdot}6$, $f = 30$ Hz).

It is interesting to note that region II does not re-occur at larger distances downstream for $r = 0{\cdot}4$ or $0{\cdot}3$, (figure 14), where the length of the test section should suffice to accommodate the repetition of the process. It implies that control over the mixing layer by forcing the flow at a single frequency is limited to a given wavelength associated with the particular frequency, suggesting a Strouhal number fx/U as a parameter governing the flow.

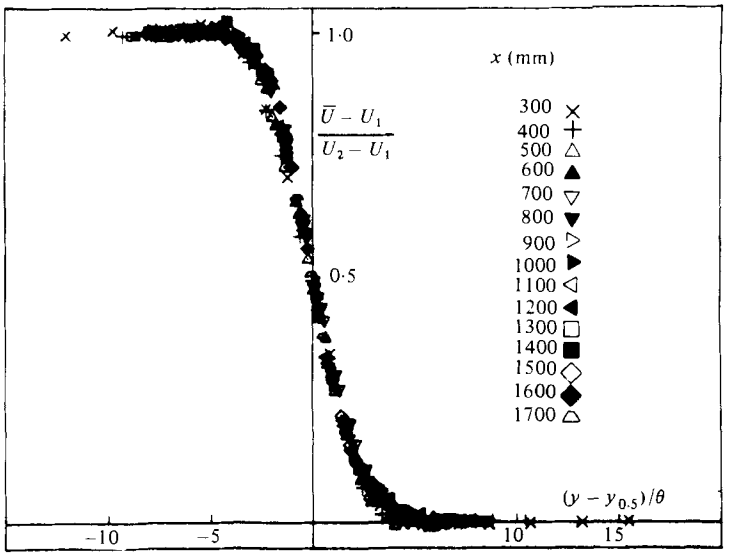

FIGURE 16. Distribution of the mean velocity in the forced mixing layer; $r = 0{\cdot}6$, $f = 30$ Hz, $A = 1{\cdot}5$ mm.

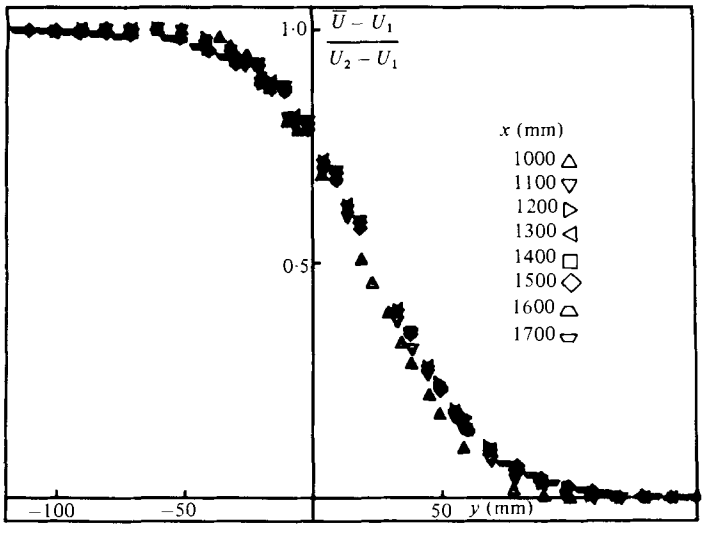

FIGURE 17. Variation of the mean-velocity profile in region II of a forced mixing layer; $r = 0{\cdot}6$, $f = 40$ Hz, $A = 1{\cdot}5$ mm.

3.4. *The mean-velocity profile*

The lateral distribution of the mean velocity in all 3 regions noted previously can be reasonably represented by an error function or by an exponential distribution of the type $\exp(-cy^2)$. In the range of forcing amplitudes considered, the shape of the mean-velocity profile does not become distorted as it did in another investigation (Wygnanski, Oster & Fiedler 1979).

In region I an increase in the forcing amplitude only broadens the mean-velocity distribution when all other flow parameters are kept constant (figure 15). The velocity profiles are reasonably similar in all three regions when the lengthscale chosen for the reduction of data is $\tilde{\eta} = (y-y_{0.5})/\theta$ (figure 16). In the truly self-similar case $\theta \propto x$ and, consequently, $\tilde{\eta} \propto \eta$. It should be stressed that in regions I and III $d\theta/dx > 0$,

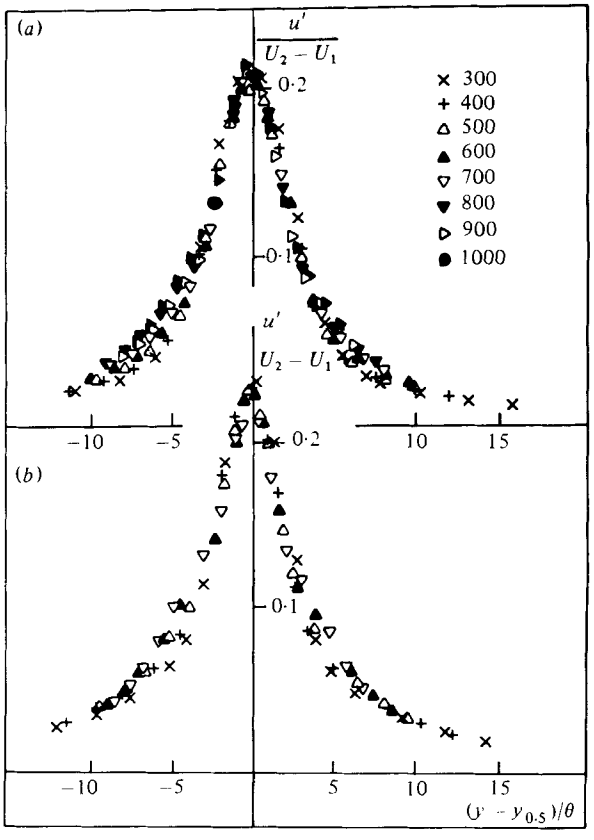

FIGURE 18. Variation of the intensity of the streamwise velocity fluctuations in region I; $r = 0{\cdot}6$, $A = 1{\cdot}5$ mm: (*a*) $f = 30$ Hz; (*b*) $f = 40$ Hz.

and hence the streamwise velocity gradient $(\partial \bar{U}/\partial x)_{y>0} > 0$ and becomes negative at $y < 0$.

In region II however, for the larger amplitudes considered, the lateral-velocity distribution does not change with x (i.e. $\partial \bar{U}/\partial x = 0$), as may be seen in figure 17 for $x > 1100$.

3.5. *The turbulent intensity*

The distribution of the streamwise component of the turbulent intensity changes from region to region.

The distribution of u' in region I has a characteristic bell shape (see figure 18*a*, *b*). However, the maximum value of $u'/(U_2 - U_1)$ depends not only on the amplitude, but also on the frequency of forcing while all other parameters are kept constant. For example

$$\{u'_{f=40\text{Hz}}/u'_{f=0}\}_{\max} = 1{\cdot}3 \quad \text{while} \quad \{u'_{f=30\text{Hz}}/u'_{f=0}\}_{\max} = 1{\cdot}2.$$

The effect of amplitude at a given frequency and velocity ratio on the distribution of u' is insignificant at small downstream distances, but becomes discernible at $x = 900$ mm (figure 19*a*, *b*).

In region II the 'bell-shaped' distribution of u' gives way to a double-peaked distribution; this is accompanied by a drop in the maximum intensity of this component, and a generation of a local minimum at small positive y (figure 20). The

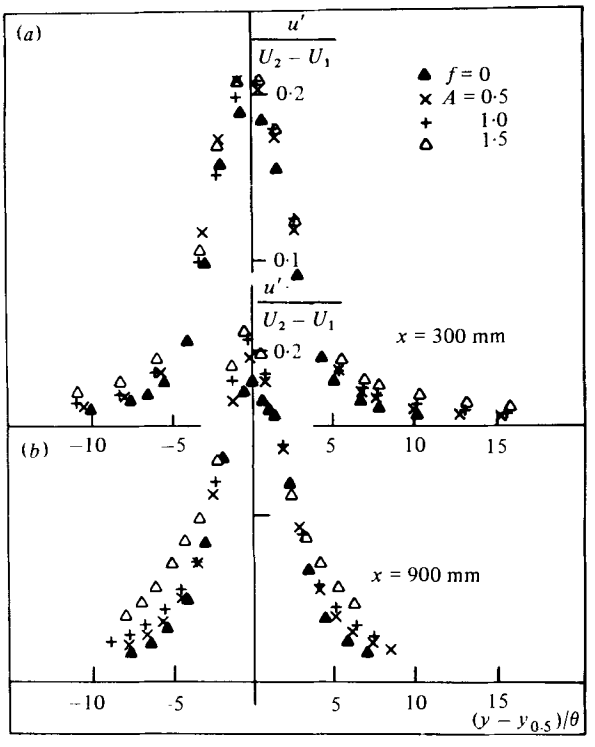

FIGURE 19. The downstream development of the distribution of the intensity of the streamwise velocity fluctuations in a forced mixing layer at $r = 0{\cdot}6$ and $f = 30$ Hz; $A = 0{\cdot}5$, 1·0, 1·5 mm: (*a*) $x = 300$ mm; (*b*) $x = 900$ mm.

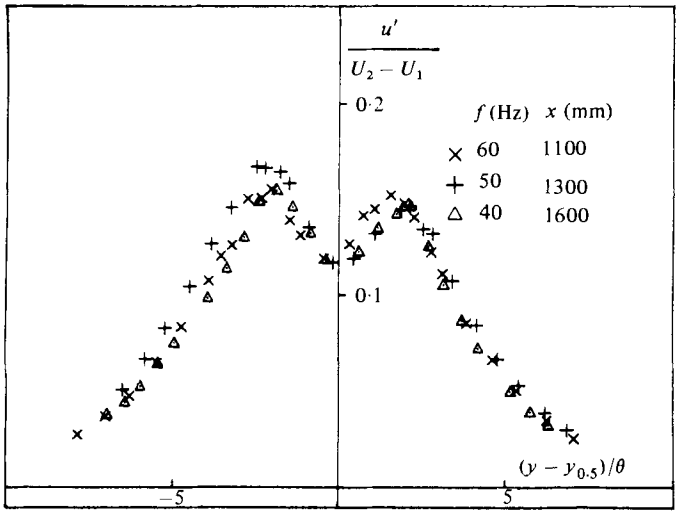

FIGURE 20. Distribution of $u'/(U_2 - U_1)$ in region II: $r = 0{\cdot}6$, $f = 40$, 50, 60 Hz.

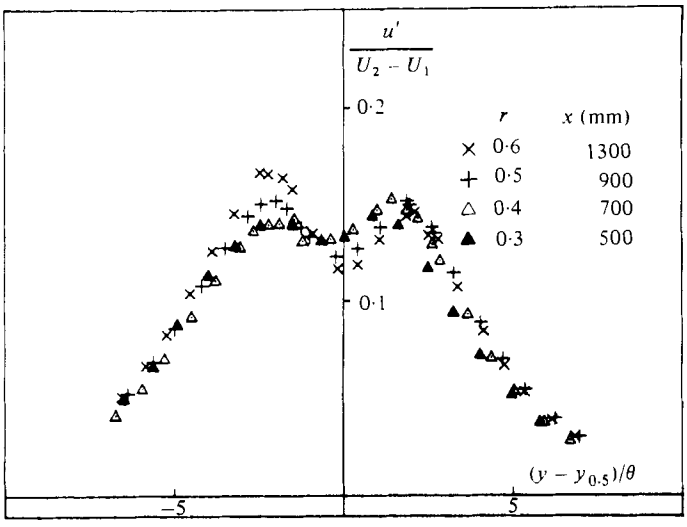

FIGURE 21. Distribution of $u'/(U_2-U_1)$ in region II; $f = 50$ Hz, $r = 0{\cdot}3$, $0{\cdot}4$, $0{\cdot}5$, $0{\cdot}6$.

twin-peaked distribution is characteristic of region II, and may be attained by changing frequency or velocity ratio while keeping the other parameters fixed (figure 21). The maximum intensity on the low-velocity side of the mixing layer ($y > 0$) is approximately constant $[u'/(U_2-U_1)]_{\max(y>0)} = 0{\cdot}15$ irrespective of r or f, the maximum intensity at $y < 0$ increases with increasing U_1/U_2 (figure 21). A similar distribution of the intensity of temperature fluctuations was observed in a slightly heated shear layer at $r = 0$ (Wygnanski, Oster & Fiedler 1979). Measurements made with rakes of resistance thermometers indicated that in region II the mixing layer consists of a row of vortex lumps crossing the measuring plane at the forcing frequency. Turbulent temperature fluctuations occurred mostly at the periphery of each lump while its core was fairly quiescent and well mixed (having an average temperature of the two streams). Provided these lumps are aligned in the lateral direction (i.e. no pairing interaction occurring in this region), they will give rise to the peculiar intensity distribution. Furthermore, if regions of strong temperature fluctuations coincide with increased u-activity, the 'double-peak' distribution of u' can be understood. It suggests that *in region II amalgamations of adjacent vortices (pairing process) are inhibited.*

The shape of the conventionally averaged, lateral distribution of v' is not affected by the transition from region I to II (figure 22), because even perfectly aligned vortex lumps with inert cores will give rise to a bell-shaped distribution of v'. The intensity of the lateral-velocity fluctuations increases rapidly with x in region I for a given velocity ratio and initial conditions. In region II, the intensity of v' remains initially constant, and even decreases somewhat further downstream (figure 22 data at $x = 1400$). The maximum intensity of $v'/(U_2-U_1)$ for the case shown is 100 % higher than in the corresponding unforced flow at the same r.

The intensity of the spanwise velocity fluctuations w' is suppressed by the introduction of periodic, two-dimensional surging (figure 23). The maximum intensity of w' decreases in region I, but remains roughly constant in region II at a level corresponding to 50 % of the unperturbed value. The suppression of the spanwise component of turbulent intensity suggests that the flow becomes more two-dimensional in response to two-dimensional forcing.

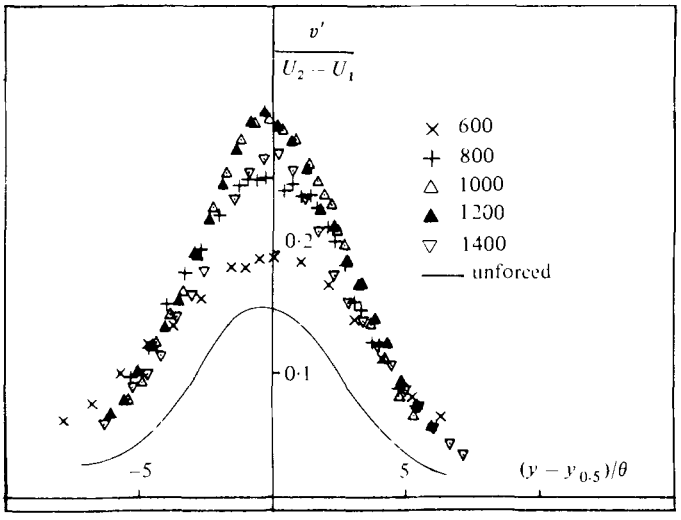

FIGURE 22. The distribution of $v'/(U_2-U_1)$; $r = 0{\cdot}6$, $f = 40$ Hz, $A = 2{\cdot}0$ mm.

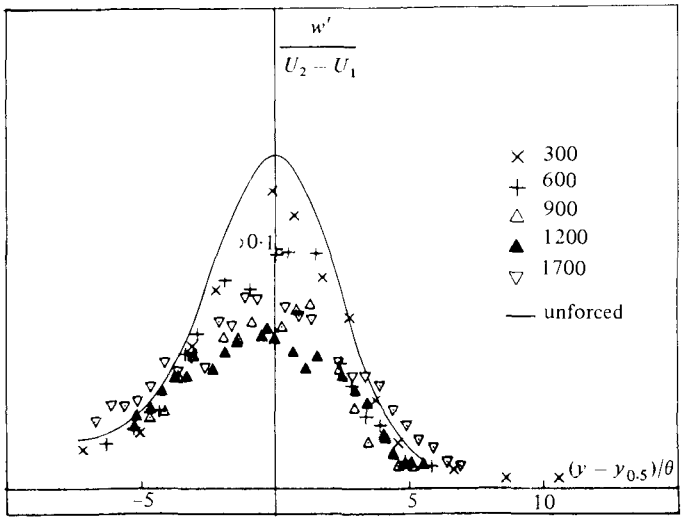

FIGURE 23. The distribution of $w'/(U_2-U_1)$; $r = 0{\cdot}6$, $f = 40$ Hz, $A = 2{\cdot}0$ mm.

It was previously observed (Wygnanski, Oster & Fiedler 1979) that the total turbulent intensity integrated across the shear layer does not change appreciably under the influence of forcing: it is simply redistributed in a manner that makes the flow more orderly and more two-dimensional than it is naturally. The same cannot be said for $U_1/U_2 = 0{\cdot}6$, where $\int_{-\infty}^{\infty}(u'^2+v'^2+w'^2)\,dy$ increased appreciably in relation to the unperturbed flow. The data shown in figure 24 are scaled by the momentum thickness at $x = 300$ (i.e. a constant length); thus the total turbulent intensity at every cross-section of the flow in the unforced case increases linearly with x. A similar trend is observed in region I, but the rate of increase of the total turbulent energy is enhanced. In region II the total turbulent intensity decreases until it becomes comparable to the intensity in the unforced case: the distribution of the intensity among the various components is still quite different from the distribution in the unforced case.

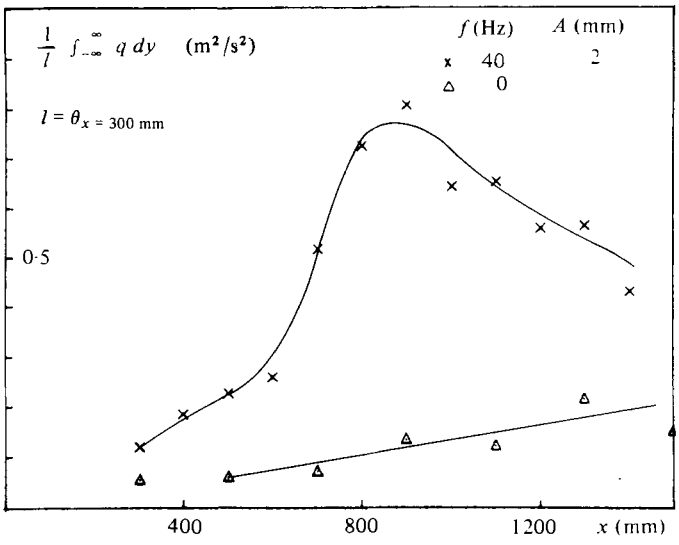

FIGURE 24. Variation of total turbulent energy in the forced mixing layer.

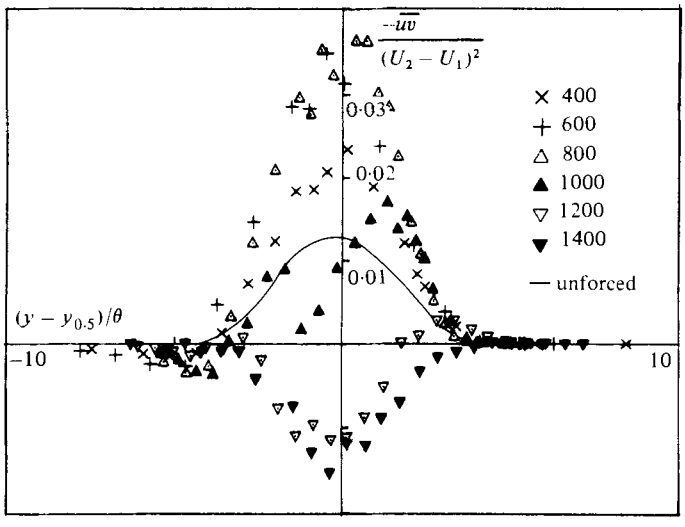

FIGURE 25. The distribution of the Reynolds stresses in a forced two-stream mixing layer; $r = 0{\cdot}6, f = 40$ Hz, $a = 2{\cdot}0$ mm.

3.6. *The Reynolds stress*

The distribution of $\overline{uv}/(U_2-U_1)^2$ in the absence of forcing has a familiar shape which correlates clearly with the lateral gradient of the mean-velocity profile (i.e. $[-\overline{uv}/(U_2-U_1)^2]_{\max} = 0{\cdot}013$ coincides with the location at which $\partial\overline{U}/\partial y$ is maximum). The lateral distribution of the shear stress in the forced mixing layer is entirely different (figure 25). In region I the distribution of $-\overline{uv}$ is entirely positive, but its maximum value increases with downstream distance. At $x = 800$ mm (for $r = 0{\cdot}6, f = 40$ Hz) $[-\overline{uv}/(U_2-U_1)^2]_{\max} = 0{\cdot}036$, which is almost 3 *times larger* than the corresponding unforced value. At $x = 1000$ mm, the lateral distribution of the shear stress has a saddle point near $y = 0$; it remains, however, entirely positive,

with a maximum on the low-speed side of the shear layer equivalent to $-\overline{uv}/(U_2-U_1)^2 = 0{\cdot}017$.

At $x > 1200$ mm (in region II) *the shear stress changes sign* everywhere across the flow, the correlation with the mean-velocity profile becomes negative because $-\overline{uv}/(U_2-U_1)^2 = -0{\cdot}015$ coincides roughly with the location at which $\partial\overline{U}/\partial y$ is still maximum.

The distribution of Reynolds stress may be calculated directly from the mean-momentum equation, which in the absence of pressure gradient is given by

$$-\frac{\overline{uv}}{(U_2-U_1)^2} = \frac{1}{(U_2-U_1)^2}\int_{-\infty}^{y}\left[\overline{U}\frac{\partial\overline{U}}{\partial x}+\overline{V}\frac{\partial\overline{U}}{\partial y}+\frac{\partial}{\partial x}(u'^2-v'^2)\right]dy,$$

where $\overline{V}$ is obtained from continuity:

$$\overline{V} = -\int_{-\infty}^{y}\frac{\partial\overline{U}}{\partial x}dy + V_{-\infty}.$$

Having measured the streamwise component of velocity $\overline{U}$ and the turbulent intensities u' and v' at close x- and y-intervals, the distribution of $\overline{uv}$ can be calculated from the above equations provided that $V_{-\infty}$ or $\overline{V}$ at any other known location is known. Townsend (1976) chose for the self-preserving mixing layer a co-ordinate system in which $\overline{V}(\eta = 0) = 0$, which automatically locates the maximum value of $-\overline{uv}$ at $y = 0$. According to Townsend (1976, p. 203) the value of the streamwise velocity component on the axis is $\overline{U}(0) = 0{\cdot}68(U_2-U_1)$. Browand & Latigo (1979) calculated $\overline{V}$ without this constraint, but required two additional inputs in their calculations; $dy_{0{\cdot}5}/dx$ and $d\theta/dx$ in addition to the assumption of self-preservation.

The calculated results of Browand & Latigo show that $\overline{V} = 0$ at $(y-y_{0{\cdot}5})/\theta = 2$, corresponding to $\overline{U} = 0{\cdot}15(U_2-U_1)$, while $\overline{uv}$ has a maximum at $(y-y_{0{\cdot}5})/\theta = -0{\cdot}5$, corresponding to $\overline{U} = 0{\cdot}6(U_2-U_1)$, whenever the boundary layer on the splitter plate is laminar. The results for the turbulent initial conditions do not differ substantially. In this investigation $V_{-\infty}$ was calculated by adding the continuity equation to the momentum equation and integrating across the entire shear layer, which results in

$$\int_{-\infty}^{\infty}\frac{d}{dx}\overline{U}^2dy + U_1V_{\infty} - U_2V_{-\infty} + \frac{d}{dx}\int_{-\infty}^{\infty}(u'^2-v'^2)\,dy = 0.$$

After substituting for $V_{\infty} = -\int_{-\infty}^{\infty}(\partial\overline{U}/\partial x)\,dy + V_{-\infty}$ the normal velocity component on the high-speed side outside the mixing layer becomes

$$\frac{V_{-\infty}}{U_2-U_1} = \frac{1}{(U_2-U_1)^2}\int_{-\infty}^{\infty}\frac{d}{dx}\left[(\overline{U}-U_1)\,\overline{U}+u'^2-v'^2\right]dy.$$

This permits the calculation of $\overline{V}$ and $\overline{uv}$ from measurements of the streamwise components of velocity and turbulence intensity without resorting to additional assumptions.

Although it is customary to neglect the term $\partial(u'^2-v'^2)/\partial x$ in many calculations (e.g. Townsend 1976, p. 192; Browand & Latigo 1979) only this term can be responsible for inverting the sign of the Reynolds stresses whenever $d\overline{U}/dx$ vanishes in region II (figure 17). Thus in region II the lateral velocity

$$\overline{V} \approx V_{-\infty} \approx \int_{-\infty}^{\infty}\frac{d}{dx}\left(\frac{u'^2-v'^2}{U_2-U_1}\right)dy$$

is almost constant across the flow. In practice, the term $\overline{U}\partial\overline{U}/\partial x$ is of the same order of magnitude as $\partial(u'^2-v'^2)/\partial x$ and $\overline{V}\partial\overline{U}/\partial y$ because even a minute contribution to $\partial\overline{U}/\partial x$ becomes substantial when multiplied by $\overline{U}$.

The distribution of $\overline{uv}$ was calculated and compared with the experimental data for $r = 0{\cdot}6$, $f = 40$ Hz and $A = 2$ mm. The calculations are very sensitive to the choice of $V_{-\infty}$; changing $V_{-\infty}/(U_2-U_1)$ by 0·001 will give a finite value of $\overline{uv}$ at $y \to \infty$. The calculated distribution of $\overline{uv}$ presented in figure 26 was obtained by forcing $(\overline{uv})_{y\to\infty} = 0$. A comparison between the calculated $V_{-\infty}$ and the one used in calculating $\overline{uv}$ is shown in figure 27; the variation of both quantities with x is similar. The difference between the calculated $V_{-\infty}$ and the $V_{-\infty}$ required for convergence of $\overline{uv}$ may stem from making use of the boundary-layer approximation, in particular the assumption letting $\partial p/\partial y = 0$. It is recognized that the streamlines of the low-velocity flow (outside of the turbulent region) are curving as a result of entrainment by the high-speed flow. Although the streamwise component of velocity outside the mixing region was maintained constant by adjusting the test-section walls, such adjustments could have easily imposed lateral velocities whose magnitude is 0·01 (U_2-U_1). The calculated $\overline{uv}$ agree only qualitatively with the measured results owing to cumulative errors caused by substracting large numbers, nevertheless the agreement is sufficiently good to give confidence in the measurement.

Integrating the production of turbulent kinetic energy across the flow,

$$\frac{1}{(U_2-U_1)^3}\int_{-\infty}^{\infty}\left[\overline{uv}\frac{\partial\overline{U}}{\partial y}+(u'^2-v'^2)\frac{\partial\overline{U}}{\partial x}\right]dy,$$

at the various downstream locations shows (figure 28) that the net production for $x > 1100$ mm is negative.

Knight (1979) and Riley & Metcalfe (1980) presented results simulating the temporal evolution of a forced mixing layer. Riley & Metcalfe predicted the existence of negative Reynolds stresses as well as negative production of turbulent kinetic energy. Part of their results agree only qualitatively with the present measurements, because the simulation was made with different initial conditions. Zaman & Hussain (1980) observed negative shear stresses in the mixing layer of a forced axisymmetric jet, which occurred 'especially during pairing'. The present results would indicate that the negative Reynolds stresses are associated with region II in which pairing is inhibited. Wygnanski, Oster & Fiedler (1979) identified the negative $-\overline{uv}$ product with the phase locked $\langle uv\rangle$-correlation, suggesting that at least a fraction of the negative Reynolds stress is produced by the large coherent eddies passing the points of measurement at the fundamental forcing frequency. The negative Reynolds stresses may be associated with the inclination of the large eddies, as proposed by Browand (1980).

4. Discussion

4.1. *The large coherent structures and their relation to the growth of the mixing layer*

A smoke filament was introduced at the trailing edge of the splitter plate and was photographed with the aid of a flash at $U_1/U_2 = 0{\cdot}4$. In the unforced case, the smoke is concentrated in discrete lumps, whose size increases with downstream distance (figure 29). Approximately 350 mm downstream of the splitter plate the distance between adjacent lumps of smoke is 63 mm (i.e. $\Lambda = 63$ mm). The distance between adjacent lumps of smoke increases with x and is an integral multiple of Λ (figure 29).

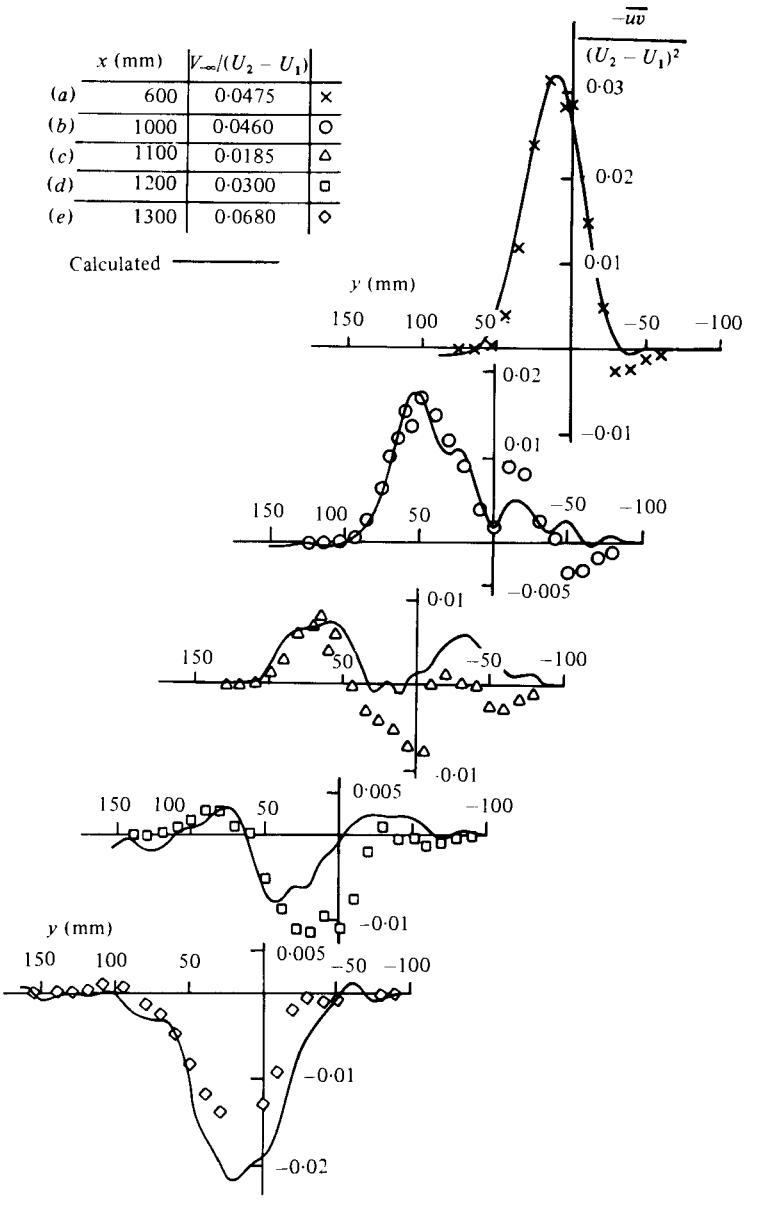

FIGURE 26. Reynolds stresses calculated by integration of the momentum equation: (*a*) $x = 600$ mm; (*b*) 1000 mm; (*c*) 1100 mm; (*d*) 1200 mm, (*e*) 1300 mm.

The length Λ is not necessarily the fundamental wavelength of the eddies shed at the trailing edge of the splitter plate because these eddies are comparable to the thickness of the smoke filament. Oster *et al.* (1977) observed that the predominant frequency near the splitter plate at $U_1/U_2 = 0{\cdot}4$ was 460 Hz, which can be transformed to a wavelength of 21 mm by using the measured convection speed; this would imply that the distance between adjacent smoke filaments is an integral multiple of the predominent wavelength existing at the intitiation of the mixing process. Furthermore, it suggests that the mixing layer spreads laterally by an amalgamation of these

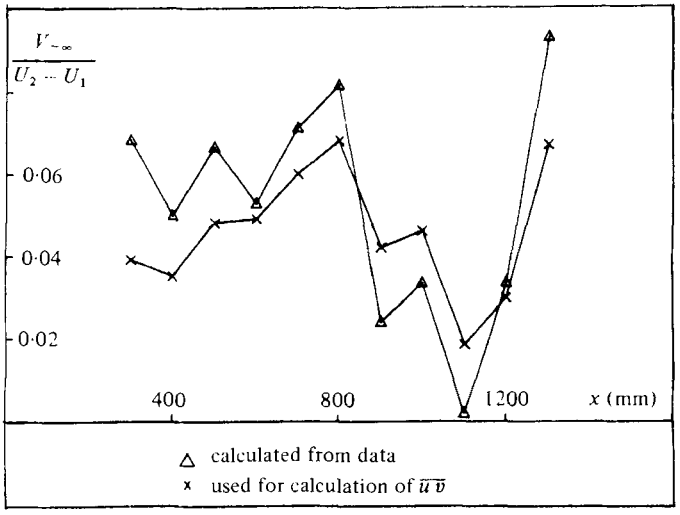

FIGURE 27. Distribution of $V_{-\infty}$ in the forced mixing layer.

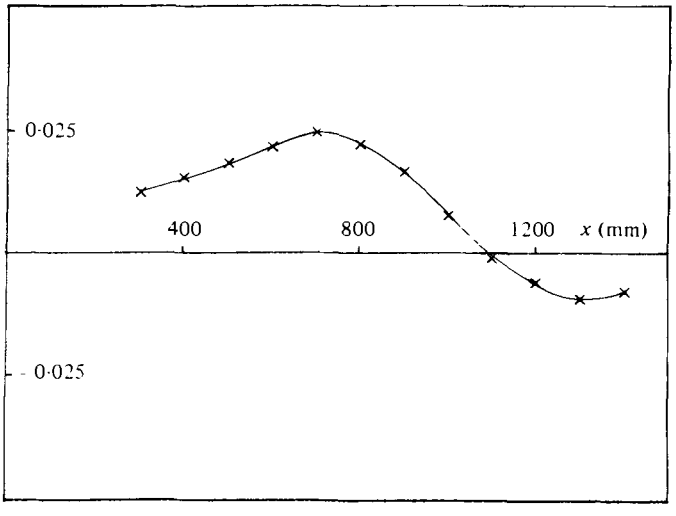

FIGURE 28. Total turbulent production across the forced mixing layer.

vortex lumps. The observation is in agreement with earlier observations of Brown & Roshko (1974) and Winant & Browand (1974). The amalgamation process must naturally occur randomly in space or time in order to give rise to smoke filaments whose scale in the particular photograph shown is Λ, 2Λ, 2Λ, 3Λ, 4Λ; furthermore, it may not necessarily involve just a pairing process of two adjacent structures. Power spectra measured outside the shear layer by Oster *et al.* (1977) at $U_1/U_2 = 0{\cdot}4$ indicate that considerable energy at $x = 500$ mm is concentrated at frequencies 460/40, 460/10, 460/8, 460/5; however, at $x = 1100$ mm the dominant frequency is 460/40. (figure 30). *The forcing frequencies selected in this experiment are in the same range as the predominant frequencies existing naturally in the flow over most of the test section.*

The physical process by which the mixing layer spreads in region I can be understood by observing temporal records of velocity taken just outside the turbulent

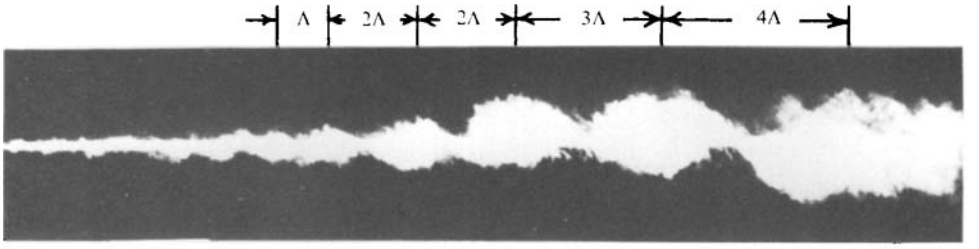

(*a*)

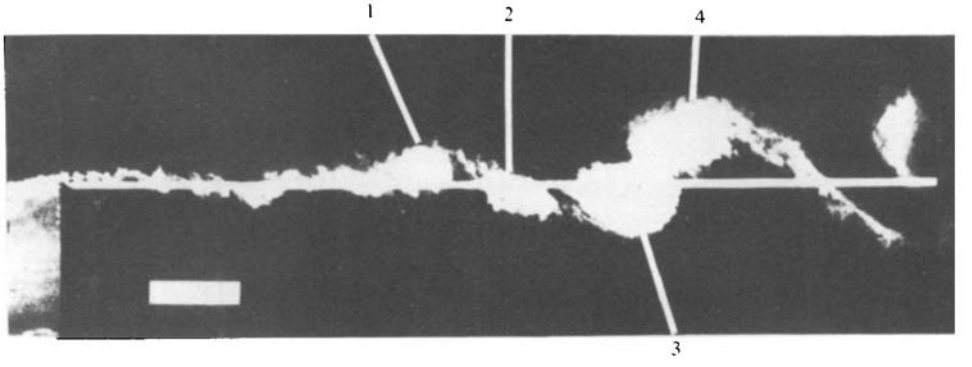

(*b*)

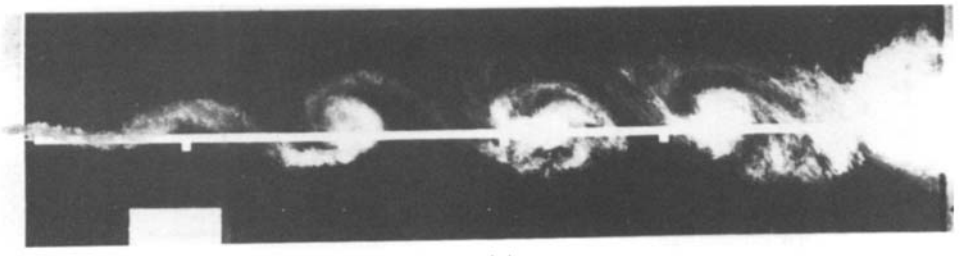

(*c*)

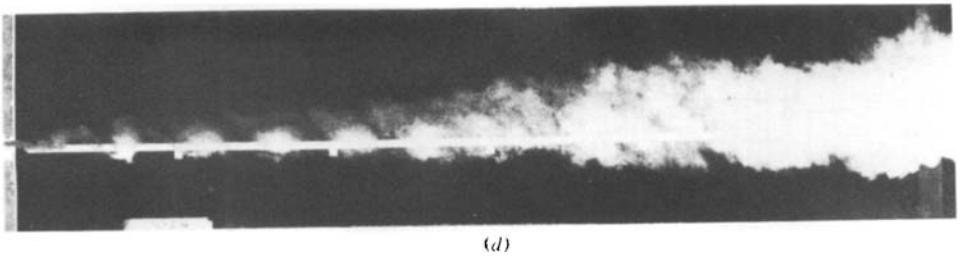

(*d*)

FIGURE 29(*a–d*). For caption see p. 118.

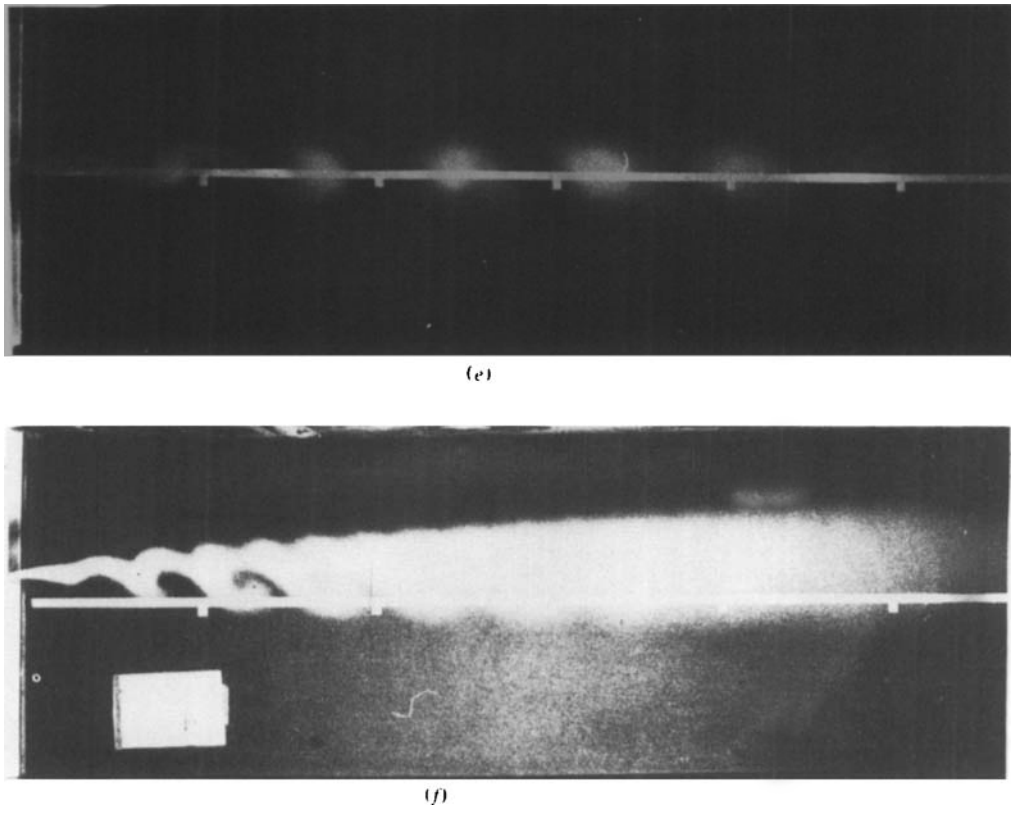

FIGURE 29. Smoke visualization of a mixing layer at $r = 0{\cdot}4$; forced at: (*a*) $f = 0$, (*b*) 20 Hz; (*c*) 40 Hz; (*d*) 100 Hz; (*e*) 60 Hz; (*f*) 100 Hz.

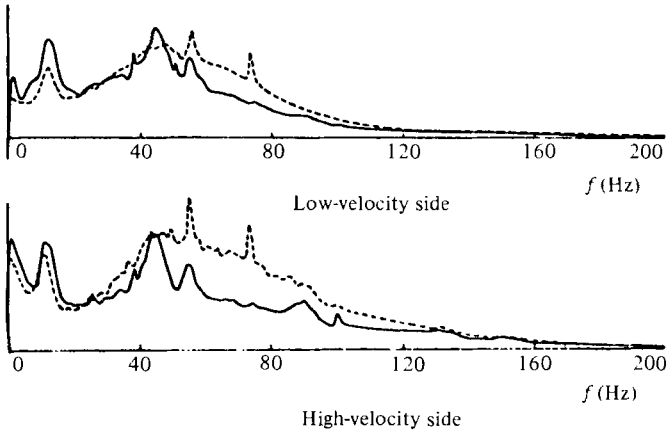

FIGURE 30. Frequency spectra in the unforced mixing layer at $x = 500$ mm; from Oster *et al.* (1977).

region at various distances from the initiation of mixing (figure 31). At these locations, the large eddies induce potential fluctuations, which are not buried in the 'noise' produced by the smaller-scale turbulence. Regular high-frequency oscillations are superimposed on the forcing frequency at $x = 300$ mm. Further downstream ($x > 400$) the appearance of the high-frequency oscillations is less regular, and is

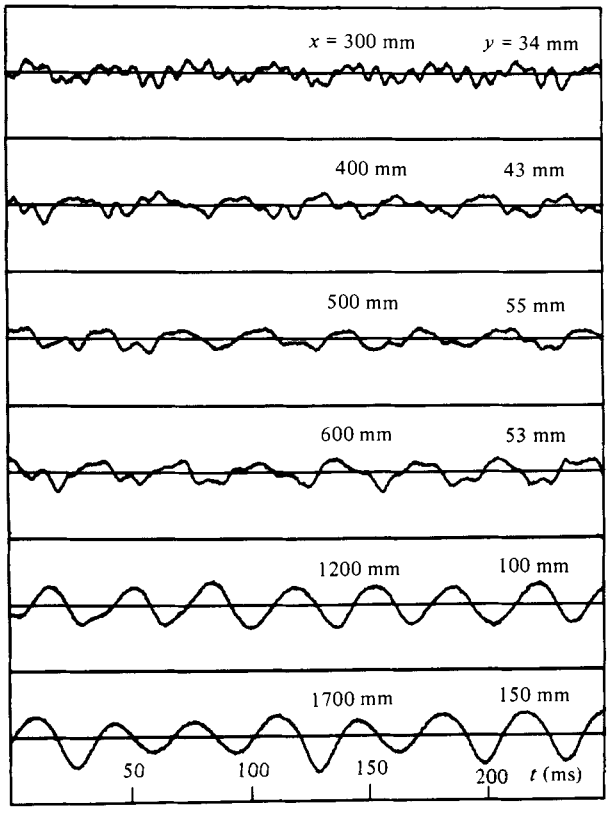

FIGURE 31. Instantaneous 'potential' velocity fluctuations induced by the large eddies within the mixing layer; $r = 0{\cdot}6$, $f = 30$ Hz, $A = 1{\cdot}5$ mm.

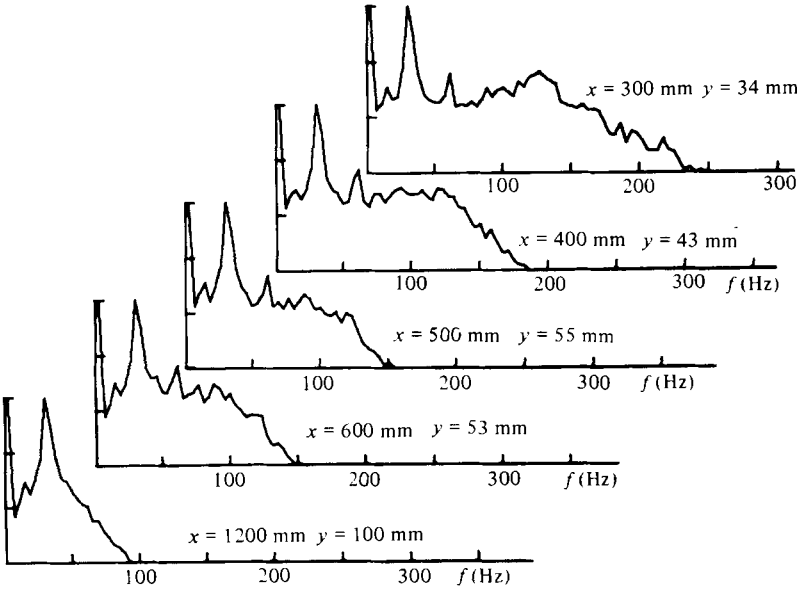

FIGURE 32. Frequency spectra of the fluctuations of figure 31.

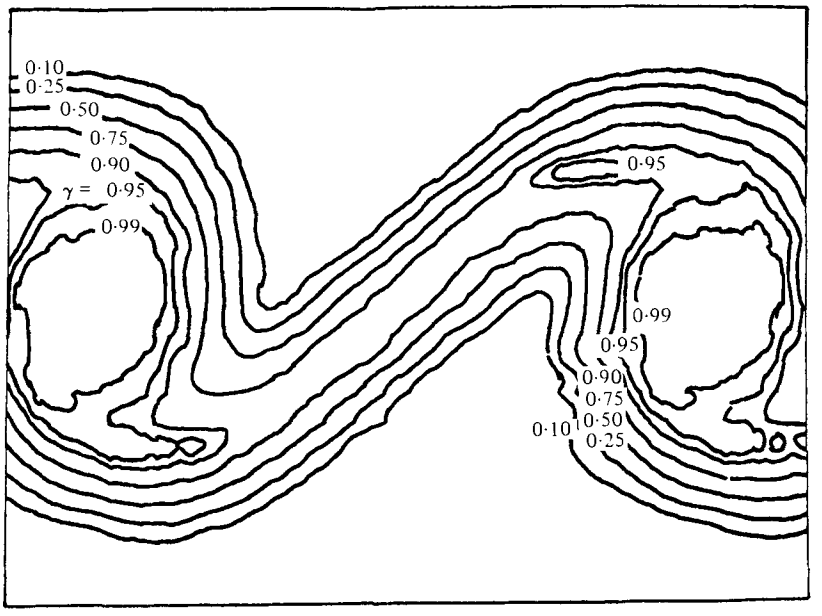

FIGURE 33. Contours of phase-averaged intermittency across the mixing layer; $r = 0{\cdot}6$, $f = 40$ Hz, $A = 1{\cdot}5$ mm, $x = 1100$ mm.

manifested by distorted patterns of the forcing frequency (e.g. $x = 600$). At $x > 1200$, periodic velocity oscillations at the forcing frequency dominate the temporal record. Power spectra of the signals just discussed are plotted in figure 32. The vertical scale in this figure is logarithmic, and the spectrum is normalized by its peak value. At $x = 300$ mm the signal is rich in harmonics of the basic frequency, which slowly diminish with increasing x until they disappear at $x = 1200$ mm.

A smoke filament photographed in region I ($r = 0{\cdot}4$, $f = 20$ Hz) confirms the interpretation of the velocity record. In the centre of the photo (figure 29*b*) two lumps of smoke (labelled 1 and 2) are perturbed by the forcing whose wavelength is approximately 500 mm. Further downstream lumps 3 and 4 are in the midst of a pairing process.

Pictures of smoke filaments taken at $U_1/U_2 = 0{\cdot}4$ and $f = 40$ Hz show an orderly array of eddies for $500 < x < 1000$ mm (figure 29*c*); pictures taken at a forcing frequency at 100 Hz show similar trains of eddies extending from $x = 200$ mm to $x = 400$ mm (figure 29*d*). For the given flow conditions, these distances correspond to the location at which the growth of the mixing layer either slows or stops entirely (region II). It is thus suspected that there are *no vortex interactions* in region II. Using stroboscopic illumination that is synchronized with the flap motion and exposing the film for 1 s indicates the region in which the large eddies are locked to the forcing frequency (figure 29*e*). In the case shown, $f = 60$ Hz, for which region II corresponds to $400 < x < 800$ mm. Vortex amalgamations occurring in this region would have caused the picture to blur. Similar pictures taken at other flow conditions (e.g. figure 29*f*) lead us to conclude that *large-eddy amalgamations are inhibited in region II.*

Temporal velocity records taken across the shear layer in region II together with phase information of the flap can supply additional evidence backing up the suggestion that the pairing process is inhibited in this region. The time of occurrence of the turbulent–non-turbulent interface was determined for each temporal record,

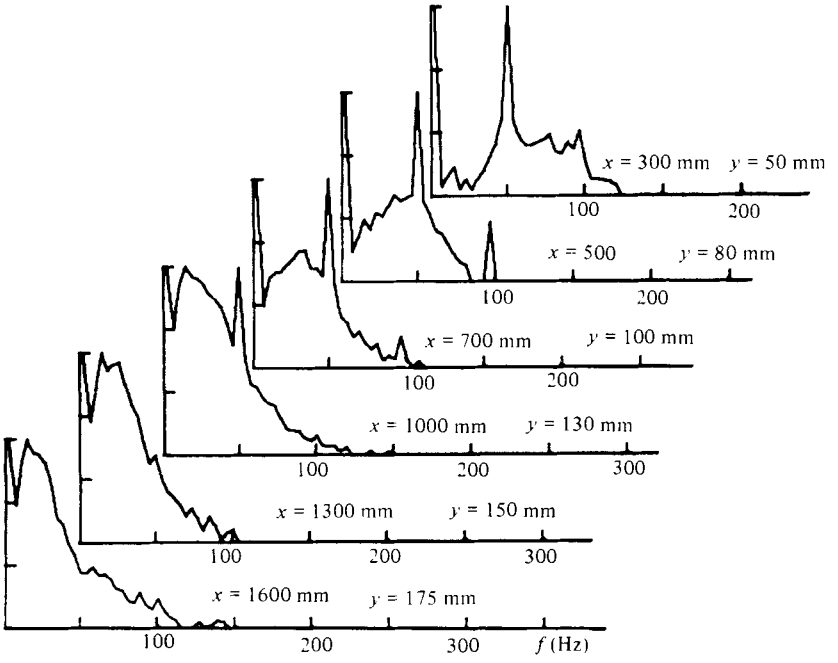

FIGURE 34. Evolution of the frequency spectra along the low-speed side of the mixing layer; $r = 0{\cdot}4$, $f = 50$ Hz, $A = 1{\cdot}5$ mm.

which in turn was phase-locked to the oscillation of the flap. The process was repeated over many events, providing a phase-averaged intermittency count, which was plotted in figure 33. The abscissa in this figure is time, while the ordinate corresponds to the lateral distance y. Since the convection velocity of these eddies on both sides of the shear layer varies only slightly (Oster *et al.* 1977) one may replace t by $x = 0{\cdot}5(U_1 + U_2)t$. The fully turbulent region consists of an elliptically shaped eddy, which is connected to its neighbours by a relatively thin turbulent sheet. Although the phase-averaged intermittency representation incorporates differences in the size, orientation and time of arrival to the eddies, the unmistakable shape of the contours can only come out provided there are no amalgamations in this region.

Amalgamations of adjacent eddies re-occur in region III, as may be inferred from figures 29 (d, f) and from intermittency contours, which became totally blurred in this region; but the best proof of their occurrence can be deduced from spectral analysis of potential fluctuations existing outside of the shear layer. A case in point is the group of data taken at $U_1/U_2 = 0{\cdot}4$ and $f = 50$ Hz (figure 34). At $x = 300$ mm (corresponding to region I) most of the energy is contained in frequencies that are higher than the forcing frequency. At $x = 500$ mm (corresponding to region II) most of the energy is centred around the forcing frequency. At $x > 700$ (corresponding to region III) the energy content shifts towards lower frequencies, attaining a broad peak in the vicinity of the first subharmonic frequency at 25 Hz. The shift of energy towards the subharmonic frequency suggests that amalgamations re-occur. The fact that the power spectrum at $x > 1300$ mm is fairly broad implies that the amalgamations occur at random and are most probably not limited to pairings alone.

The shear layer appears to regain its linear growth in region III, as may be seen in figure 14. Thus the considerations of self-preservation may be applied to this region.

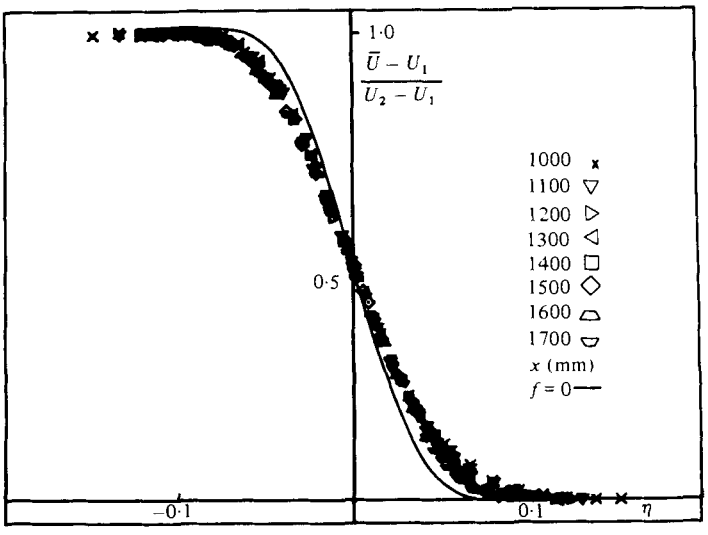

FIGURE 35. Distribution of the mean velocity in the far field; $r = 0{\cdot}4$, $f = 50$ Hz, $A = 1{\cdot}5$ mm.

A more interesting question is the universality of the concept for the asymptotic case at $x \to \infty$. In figure 35 the mean-velocity profile is drawn for the forced mixing layer using the familiar similarity co-ordinates $\eta = (y-y_{0{\cdot}5})/(x-x_0)$, where x_0 is the virtual origin of the flow. The velocity distributions measured at various x-stations scale as well in this co-ordinate system for the forced mixing layer as they do for the unforced one, provided one selects the appropriate x_0 for each case. The spreading rate of the forced flow is quite different from the natural case shown for comparison in figure 35. The streamwise component u' of the turbulent fluctuations, when plotted in the same co-ordinates and compared with the unforced case, indicates that even in region III the maximum value of $u'/(U_2-U_1)$ is higher and the distribution of u' is wider (figure 36). Thus the *universality of self-preservation for the two-dimensional mixing region becomes questionable*. One may consider either similarity limited to a specific experiment or a local similarity achieved by using a local characteristic lengthscale (e.g. θ) for the purpose of normalization. This may contradict some of the experiments of Fiedler & Thies (1978) concerned with the universality of the self-preserving region.

4.2. *Possible theoretical implications*

It seems that a relationship among time-averaged variables cannot account for the large effect that the periodic forcing has on the development of the flow. Thus it would appear that theoretical models relying on the equation for the Reynolds stress and a balance of turbulent energy would not be applicable in this case. Furthermore, a simple closure assumption relating the mean-velocity profile or the distribution of turbulent energy to the distribution of Reynolds stress will not give the correct answer either. Laufer (1980, private communication) in discussing deterministic versus stochastic approaches to turbulence suggests that 'small-scale motions do not play an important role in the dynamics of flow development...and the turbulent energy balance is a consequence and not the driving mechanism of turbulent transport.' It would appear that the large eddies are responsible for the peculiar behaviour of this flow.

Direct numerical simulation in which the governing equations of motion are solved

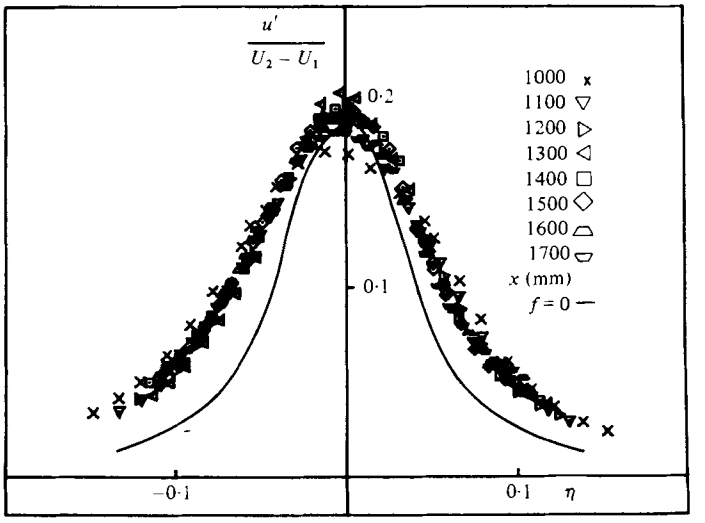

FIGURE 36. Distribution of the streamwise velocity fluctuations in the far field; $r = 0{\cdot}4$, $f = 40$ Hz, $A = 1{\cdot}5$ mm.

may provide some answers to the physical aspects of the problem provided that the Reynolds number is fairly small or its effects on the flow are negligible. At high Reynolds number, closure assumptions are still necessary for the small-scale motions. The perturbed turbulent mixing layer was simulated numerically by Riley & Metcalfe (1980). The results of the simulation agree qualitatively with the findings discussed in this paper. The presence of subharmonic oscillations is required in order that the vortices, at the perturbation wavelength, will roll around one another and cause the shear layer to spread laterally. In the absence of the subharmonic frequency, vortex amalgamations are impeded, resulting in negative turbulence production, and an inhibition of the growth of the mixing layer. Riley & Metcalfe suggest that a particularly strong coupling between the perturbation frequency and its subharmonic exists when the latter is a quarter of a wavelength out of phase with the former, enhancing the lateral spread of the flow. A similar conclusion was reached by Patnaik, Sherman & Corcos (1976) in their computer simulation. A phase shift between the subharmonic and the fundamental resulted in a 'rolling interaction', whereas a 'shredding interaction', in which no rolling was observed, occurred at other instances. This configuration is currently being studied experimentally in Tel-Aviv. Computer simulations are analogous to laboratory experiments because they do not tell the investigator *a priori* which of the flow variables dominate a given configuration, while a theoretical analysis contains the possibility of prediction. Riley & Metcalfe predicted the occurrence of region II in their numerical simulation. They chose time as their independent variable, and defined a parameter $T\Delta U/\Lambda$ to be of importance. Here T is the time elapsed from the start of the computation, ΔU is the velocity difference between the streams, and Λ is the wavelength of the perturbation.

The spatially growing mixing layer may be related to the temporal evolution of the flow by letting $TU_c = x_s$, where $U_c = \frac{1}{2}(U_1 + U_2)$ represents the convection velocity of the large eddies (Oster *et al.* 1977), x_s is the distance between the centre of region II and the splitter plate, and $\Lambda = U_c/f$. Hence the parameter $T\Delta U/\Lambda = 2\lambda x_s f/U_c$, which is a Strouhal number multiplied by a dimensionless velocity ratio $\lambda = (U_2 - U_1)/(U_2 + U_1)$. For all cases studied, the centre of region II occurs

approximately at $\lambda x_s f/U_c = 1{\cdot}5$. Region II starts at $\lambda xf/U_c = 1$ and ends at $\lambda xf/U_c = 2$.

Fiedler (1980) discusses the evolution of periodic disturbances in a plane shear layer at $r = 0$. The periodic content of the lateral fluctuations v at the excitation frequency f was examined: its first harmonic ($2f$) and its first subharmonic ($0{\cdot}5f$) were measured along the x-axis and analysed for two different forcing frequencies ($f = 20$ Hz and $f = 40$ Hz). The downstream amplification of the oscillations at the excitation frequency was approximately two orders of magnitude, while the harmonic and subharmonic frequencies were amplified to a much lesser degree. The amplification rates are compared with Michalke's (1965) inviscid stability theory and found to agree very well with the predicted amplification rates (figure 37). These results confirm the proposition that the large coherent structures in the mixing layer may be governed by an inviscid process. This behaviour of the flow was suspected for quite some time, leading to calculations based on the interaction of arrays of inviscid vortices that were slightly perturbed in the lateral direction (Ashurst 1977; Delcourt & Brown 1979). The calculations predict the growth of the mixing layer, and the coalescence of the vortices into discrete, large clouds. More surprising is the fact that linear stability theory predicts so well the amplification of fluctuations that are not infinitesimal in their amplitude. Furthermore, at the distance at which the artificially excited modes attained their maximum amplification, the initially unstable modes prevailing near the splitter plate had undergone a number of amalgamations, which are considered to be a result of a nonlinear process. This would imply that the amplification resulting from linear inviscid instability is not disturbed by amalgamation of smaller vortices. One may easily accept this notion provided there is a large disparity of scales between the vortices shed at the trailing edge of the splitter plate, and the wavelength associated with the forcing frequency ($f_{\text{initial}}/f_{\text{forcing}} \approx 10$). It seems less acceptable in relation to the first harmonic or subharmonic of the forcing frequency. Fiedler (1980) extended the application of Michalke's theory to non-parallel flows by assuming that the amplification rate is given by

$$A_x/A_0 = \exp \int_0^x -\alpha_i \, dx,$$

where A_0 is the initial amplitude of the disturbance, A_x is the local amplitude of the disturbance, and α represents the spatial growth rate of the disturbance, and that the local momentum thickness θ increases linearly with x: $\theta = 0{\cdot}035x$. The assumption may be questioned, since it does not adhere to the original assumption for which the flow was calculated (i.e. θ = constant).

Another salient feature of Michalke's (1964) theory that could be tested in the present context is the distribution of vorticity. Figure 10 from Michalke's (1964) paper, which is inserted into figures 38 and 39, shows contours of constant vorticity for the most-amplified wavenumber ($\alpha = 0{\cdot}444$) and for the neutral disturbance ($\alpha = 1$) when the amplitude of the vorticity perturbation was 0·2. In the most-amplified case two maxima displaced in y are found within a single wavelength. These contours imply the existence of two parallel vortex rolls, which are displaced relative to one another and may amalgamate by rotating around each other. In the neutrally stable disturbance the vorticity distribution has only one maximum within a single wavelength.

The vorticity distribution in a turbulent mixing layer was calculated for one period of the forcing frequency corresponding to regions I and II of the flow. Phase-locked ensemble-averaged velocity profiles were calculated for $r = 0{\cdot}4$, $x = 300$ mm and a

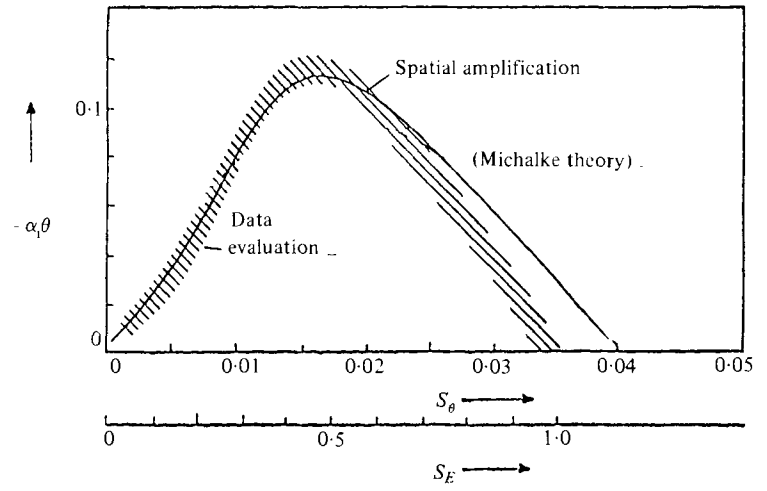

FIGURE 37. Amplification rates measured in a single-stream mixing layer compared with the theory of Michalke (1965); from Fiedler (1980).

forcing frequency of 50 Hz. The averaging process eliminates the random fluctuations occurring during each cycle, rendering the velocity profile sufficiently smooth to permit the calculation of phase-locked velocity gradient $\partial\langle U\rangle\,\partial y$. Contours of phase-locked $\partial\langle U\rangle\,\partial y$, which constitute the major contribution to spanwise vorticity, are plotted for a single cycle in figure 38. They show very clearly the required concentration of vorticity predicted by Michalke. The same procedure applied at the beginning of region II of the flow ($x = 700$ mm, $r = 0{\cdot}4$, $f = 50$) or at the centre of this region ($x = 1100$ mm, $r = 0{\cdot}6$, $f = 60$) indicates that only a single row of vortices is present in the flow during each period (figure 39).

The prevailing value of the parameter $2f\theta/U_c = f\theta/(U_2 + U_1)$ existing in region II is between 0·036 to 0·041 (figure 13). The theoretically predicted value for the neutrally stable spatial amplification is 0·04 (Michalke 1972). Thus the initial spreading rate of the forced turbulent mixing layer is related to the linear stability theory. It would require a much more detailed experiment to verify the extent of the applicability of the inviscid linear stability theory to the fully turbulent shear flow, but these results are sufficiently encouraging to warrant such an investigation.

Crow & Champagne (1971), who artificially excited a jet, concluded that an axisymmetric wave amplifies as a result of a linear stability of a top-hat velocity profile, but saturates under the nonlinear action of a harmonic. They found no explanation based on the linear stability theory distinguishing a preferred mode of frequency $f = 0{\cdot}3\,U_j/D$ (where U_j is the jet velocity and D is the diameter), which underwent the strongest amplification before saturating. They thus resorted to a nonlinear mechanism to explain the existence of the preferred mode. Crighton (1975) reconciled the results of Crow & Champagne with the linear theory of a spatially amplified axisymmetric mode by using a mean-velocity profile that matched the measurements 2 diameters downstream of the nozzle. He also found that the stability calculations are sensitive to the thickness ratio between the shear layer and the diameter of the jet. Thus the preferred mode observed by Crow & Champagne at a Strouhal number $St = fD/U_j = 0{\cdot}3$ is not unique; values as high as 0·5 are plausible and are consistent with experimental observations. Saturation of the frequency corresponding to $St = 0{\cdot}3$ occurs at the end of the potential core some 4 diameters downstream of the nozzle.

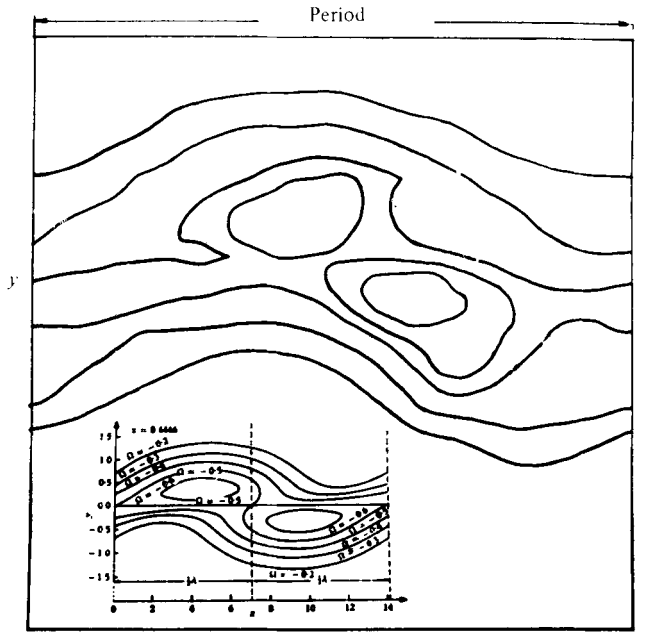

FIGURE 38. Vorticity contours calculated from the measured velocity profile in region I; $r = 0{\cdot}4$, $f = 50$ Hz, $A = 1{\cdot}5$ mm, $x = 300$ mm.

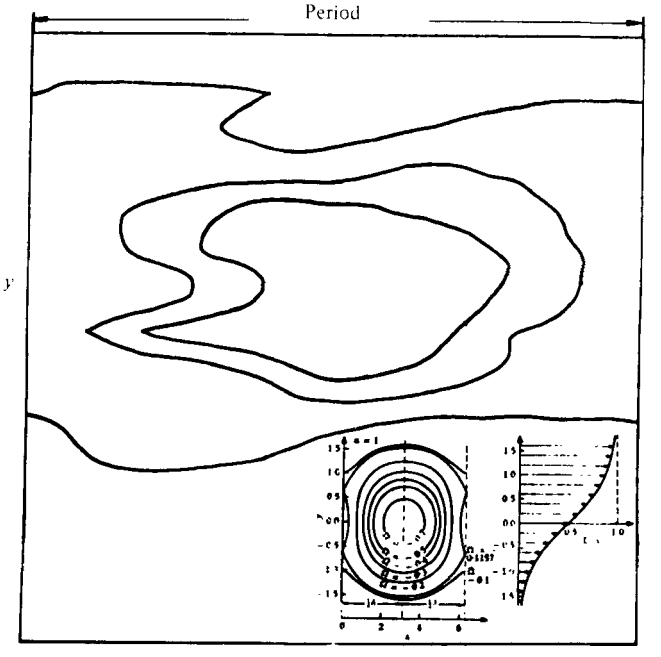

FIGURE 39. Vorticity contours calculated from the measured velocity profile in region II; $r = 0{\cdot}4$, $f = 50$ Hz, $A = 1{\cdot}5$ mm, $x = 700$ mm.

Spatial amplification predicted by the linear theory takes place in the first full wavelength of the forcing frequency (i.e. region I extends between $0 < \lambda xf/U_c < 1$). Furthermore, it takes an additional wavelength for a new instability to set in (i.e. region III starts at $\lambda xf/U_c \approx 2$). Region II is dominated by the fundamental frequency to which the mean flow is stable in the linear sense; it may also be characterized by the absence of vortex amalgamations. However, the subharmonic frequency may develop rather quickly, because it is the most unstable one in region II ($0{\cdot}018 < f\theta/(U_1+U_2) < 0{\cdot}02$). Laufer & Monkewitz (1980), after observing that the axisymmetric shear layer at the nozzle lip is already modulated by a low frequency corresponding to $St = 0{\cdot}3$, suggested that the perturbation generated by this mode propagates upstream and may influence the development of the shear layer. They conjecture that a row of two-dimensional vortices will interact with its subharmonic. The interaction results in a pairing process. This means that the total time required for a vortex to reach a pairing location and the time needed for the signal produced by the pairing to propagate upstream to the nozzle should be equal to an integer multiple of the fundamental frequency:

$$x_p\left(\frac{1}{U_c}+\frac{1}{a}\right)=\frac{N}{f},$$

where a is the velocity of sound, and x_p is the location at which pairing is initiated. Since in the present case $1/U_c \gg 1/a$, this equation implies that $x_p f/U_c = N$, provided that $U_1/U_2 = 0$ and in the general case for mixing between co-flowing streams $\lambda f x_p/U_c = N$ (see also Laufer & Monkewitz 1980).

The mechanism for the interaction of a fundamental perturbation mode in its nonlinear range was first suggested by Kelly (1967). Numerical simulations of Riley & Metcalfe (1980) and Patnaik *et al.* (1976) show that the presence of a subharmonic that is out of phase with the fundamental frequency is essential for the vortex-pairing process. When the mixing layer between two streams at $r = 0{\cdot}4$ is excited at a frequency $f = 50$ Hz its growth is inhibited at $500 < x < 1000$ mm. At $x = 500$ m, corresponding to $\lambda fx/U_c = 1$, the power spectra is dominated by the forcing frequency (figure 32), with the harmonic or the subharmonic content being two decades lower than the fundamental. At $\lambda fx/U_c = 1{\cdot}5$ the subharmonic frequency becomes apparent, although its amplitude is still one decade below the frequency of excitation. At $\lambda fx/U_c = 2{\cdot}15$ (corresponding to $x = 1000$ mm) at the beginning of region III the amplitudes of the forcing frequency and its subharmonic are equal, while at the next measuring station, corresponding to $\lambda fx/U_c = 2{\cdot}8$, only the broad subharmonic frequency dominates the flow.

Thus the subharmonic frequency that is being amplified in region II interacts with the fundamental at the beginning of region III, causing a renewed growth of the mixing layer. The phase relation between the excitation frequency and its subharmonic should be carefully examined.

It appears that one wavelength of the fundamental frequency is required for the subharmonic frequency to set in, and a similar distance is needed for completion of the amalgamation process. The measurements of Kibens (1980) also support this observation; however, on the basis of the data available to us we could not safely suggest that a feedback mechanism is responsible for the vortex amalgamation.

5. Conclusions

The two-dimensional turbulent mixing layer is very susceptible to small-amplitude periodic surging that is introduced at its origin. The rate at which the shear layer spreads laterally, the distribution of the turbulent intensity and the Reynolds stress are all affected by the forcing frequency and amplitude for a given velocity ratio between the two streams. Thus a product of the Strouhal number and a dimensionless velocity ratio $\lambda = (U_2 - U_1)/(U_2 + U_1)$ becomes an important parameter in this flow. The sensitivity of the mixing layer to small-amplitude perturbations explains the scatter in the spreading-rate parameters measured by various investigators, for otherwise identical experimental configurations. These perturbations may occur naturally as a result of vibration, blade-passage frequency, small separated regions in the diffuser, etc.

Two-dimensional oscillations of very small amplitude tend simply to increase the spreading rate of the flow, but at larger amplitudes the mixing layer resonates with the imposed oscillation in the region bounded by $1 < \lambda fx/U_c < 2$, where $U_c = \frac{1}{2}(U_1 + U_2)$ is the convection velocity of the large eddies. Flow visualization supported by velocity and temperature measurements (Wygnanski, Oster & Fiedler 1979; Wygnanski, Oster, Fiedler & Dziomba) indicates that the shear layer in this region consists of a single array of large, quasi-two-dimensional vortex lumps, which do not interact with one another. The suppression of vortex interaction results in the inhibition of the lateral growth of the shear layer, the generation of negative Reynolds stresses, and hence the extraction of energy from the turbulence to the mean motion; and finally a redistribution of the available turbulent energy.

The amalgamation of coherent eddies occurs on both sides of the resonance region. Small-scale eddies shed from the trailing edge of the splitter plate coalesce in the initial region of the flow, and their coalescence is associated with the lateral spread of the shear layer. The low frequency of the artificial excitation seems to accelerate the rate of amalgamation of these eddies and thus increase the lateral rate of spread of the mixing layer for $0 < \lambda fx/U_c < 1$. It is not apparent from this study whether (i) the artificially excited frequency acts only on its first harmonic by a feedback mechanism extending all the way to the trailing edge of the splitter plate, thus initiating a pairing process, with the first harmonic acting on the second harmonic frequency in a similar fashion giving rise to a cascade process that eventually initiates the first pairing near the trailing edge of the splitter plate; or (ii) the forced wave displaces a large number of smaller eddies and bunches them together into a large single lump. The latter process was suggested by Ho & Nosseir (1981), and is referred to as collective interaction. The dynamics of vortex coalescence should be carefully investigated in the future, but it is surprising to note that the linear inviscid stability theory is capable of predicting some important features of this flow.

Artificial excitation of the shear layer at its origin may have many engineering applications because it offers an opportunity of manipulating and controlling the turbulence and the spreading rate of this important flow. The distance over which control may be exercised depends on the *frequencies* of forcing, which in many cases may be an order of magnitude lower than the initial instability frequency near the nozzle. The turbulent mixing layer, because of its dependence on the initial conditions, may never become a universal self-preserving flow.

This work was supported in part by a D.F.G. grant in co-operation with Professor H. E. Fiedler, Technical University Berlin.

REFERENCES

ASHURST, W. T. 1977 *Sandia Lab. Rep.* SNAD 77–8613.

BATT, R. G. 1975 *A.I.A.A.* **13**, 245.

BIRCH, S. F. 1977 In *Turbulence in Internal Flows* (ed. S. N. B. Murthy), p. 89. Hemisphere.

BIRCH, S. F. 1980 In *Proc. Stanford Conf. on Complex Turbulent Flows.*

BROWAND, F. K. 1980 *Bull. Am. Phys. Soc.* **25**, 1102.

BROWAND, F. K. & LATIGO, B. O. 1979 *Phys. Fluids* **22**, 1011.

BROWN, G. L. & ROSHKO, A. 1971 Turbulent shear flows. *AGARD*-CP-93, 23–1.

BROWN, G. L. & ROSHKO, A. 1974 *J. Fluid Mech.* **64**, 775.

CHAMPAGNE, F. H., PAO, Y. H. & WYGNANSKI, I. J. 1976 *J. Fluid Mech.* **74**, 209.

CHANDRSUDA, C., MEHTA, R. D., WEIR, A. D. & BRADSHAW, P. 1978 *J. Fluid Mech.* **85**, 693.

CRIGHTON, D. D. 1975 *Prog. Aero. Sci.* **16**, 31.

CROW, S. C. & CHAMPAGNE, F. H. 1971 *J. Fluid Mech.* **48**, 547.

DELCOURT, B. A. G. & BROWN, G. L. 1979 In *Proc. 2nd Symp. on Turbulent Shear Flows, London.*

DIMOTAKIS, P. E. & BROWN, G. L. 1976 *J. Fluid Mech.* **78**, 535.

DZIOMBA, B. 1981 Ph.D. thesis D83, Technical University Berlin.

FFOWCS WILLIAMS, J. E. & KEMPTON, A. J. 1978 In *Structure and Mechanisms of Turbulence II* (ed. H. Fiedler). Lecture Notes in Physics, vol. 76, p. 265. Springer.

FIEDLER, H. E. 1980 In *Proc. Int. Conf. on Turbulent Flows, Madrid.*

FIEDLER, H. & THIES, H. J. 1978 In *Structure and Mechanisms in Turbulence I* (ed. H. Fiedler). Lecture Notes in Physics vol. 75, p. 108, Springer.

FOSS, J. F. 1977 In *Proc. 1st Int. Symp. on Turbulent Shear Flows, Penn. State University.*

GOLDSTEIN, S. 1930 *Proc. Camb. Phil. Soc.* **26**, 1.

HERNAN, M. A. & JIMENEZ, J. 1979 In *Proc. 2nd Symp. on Turbulent Shear Flows, London.*

HILL, J. C. 1976 *Ann. Rev. Fluid Mech.* **8**, 135.

HO, C. M. & NOSSEIR, N. S. 1978 *Bull. Am. Phys. Soc.* **23**, 1007.

HO, C. M. & NOSSEIR, N. S. 1981 *J. Fluid Mech.* **105**, 119.

HUSSAIN, A. K. M. F. & ZEDAN, M. F. 1978*a* *Phys. Fluids* **21**, 1100.

HUSSAIN, A. K. M. F. & ZEDAN, M. F. 1978*b* *Phys. Fluids* **21**, 1475.

KELLY, R. E. 1967 *J. Fluid Mech.* **27**, 657.

KIBENS, V. 1980 *A.I.A.A.* **18**, 434.

KNIGHT, D. 1979 In *Proc. 6th Biennial Symp. on Turbulence, University of Missouri–Rolla.*

LAUFER, J. & MONKEWITZ, P. 1980 *A.I.A.A. Preprint* no. 80–0962.

LIEPMANN, H. W. & LAUFER, J. 1947 *NACA Tech. Note* no. 1257.

LIU, J. T. C., ALPER, A. & MANKBUDI, R. 1978 In *Structure and Mechanisms in Turbulence II* (ed. H. Fiedler). Lecture Notes in Physics, vol. 76, p. 202, Springer.

MOORE, C. J. 1978 In *Structure and Mechanisms of Turbulence II* (ed. H. Fiedler). Lecture Notes in Physics, vol. 76, p. 254. Springer.

MICHALKE, A. 1964 *J. Fluid Mech.* **19**, 543.

MICHALKE, A. 1965 *J. Fluid Mech.* **22**, 371.

MICHALKE, A. 1972 *Prog. in Aero Sci* **13**, 213.

OSTER, D., WYGNANSKI, I. & FIEDLER, H. 1977 In *Turbulence in Internal Flows* (ed. S. N. B. Murthy), p. 67. Hemisphere.

OSTER, D., WYGNANSKI, I., DZIOMBA, B. & FIEDLER, H. 1978 In *Structure and Mechanisms of Turbulence I* (ed. H. Fiedler). Lecture Notes in Physics, vol. 75, p. 48. Springer.

PATEL, R. P. 1973 *A.I.A.A. J.* **11**, 67.

PATNAIK, P. C., SHERMAN, F. S. & CORCOS, G. M. 1976 *J. Fluid Mech.* **73**, 215.

PUI, N. K. & GARTSHORE, I. 1979 *J. Fluid Mech.* **91**, 111.

REICHARDT, H. 1951 *VDI-Forschungsheft* 414, 2nd edn [1st edn 1942].

RILEY, J. J. & METCALFE, R. W. 1980 *A.I.A.A. Paper* no. 80–0274.

SPENCER, B. W. 1970 Statistical investigation of turbulent velocity and pressure fields in a two stream mixing layer. Ph.D. thesis, Nuclear Engng Program, Univ. of Illinois, Urbana.

SPENCER, B. W. & JONES, B. J. 1971 *A.I.A.A. Paper* no. 71–613.

TOWNSEND, A. A. 1976 *The Structure of Turbulent Shear Flows*, 2nd edn. Cambridge University Press.

YULE, A. J. 1971 *A.R.C. R&M* 3683.

WINANT, C. D. & BROWAND, F. K. 1974 *J. Fluid Mech.* **63**, 237.

WYGNANSKI, I. 1978 In *Proc. Dynamic Flow Conference, Marseille.*

WYGNANSKI, I. J. & FIEDLER, H. E. 1970 *J. Fluid Mech.* **41**, 327.

WYGNANSKI, I., OSTER, D. & FIEDLER, H. 1979 In *Proc. 2nd Symp. on Turbulent Shear Flows, London.*

WYGNANSKI, I., OSTER, D., FIEDLER, H. & DZIOMBA, B. 1979 *J. Fluid Mech.* **93**, 325.

ZAMAN, K. B. M. Q. & HUSSAIN, A. K. M. F. 1980 *J. Fluid Mech.* **101**, 449.

ZAMAN, K. B. M. Q. & HUSSAIN, A. K. M. F. 1981 *J. Fluid Mech.* **103**, 133.